

Multisensor Data Product Fusion for Aerosol Research

Pawan Gupta, Falguni Patadia, and Sundar A. Christopher

Abstract—Combining data sets from multiple satellite sensors is a powerful method for studying Earth–atmosphere problems. By fusing data, we can utilize the strengths of the individual sensors that may not be otherwise possible. In this paper, we provide the framework for combining level 2 data products, using data from three sensors aboard the National Aeronautics and Space Administration (NASA)’s Terra satellite. These data include top-of-the-atmosphere (TOA) radiative energy fluxes obtained from the Clouds and the Earth’s Radiant Energy System (CERES), aerosol optical thickness from the multispectral Moderate Resolution Imaging Spectroradiometer (MODIS), and aerosol properties from the Multi-angle Imaging SpectroRadiometer (MISR). The CERES Single Scanner Footprint (SSF) contains the pixel level CERES TOA fluxes and the level 2 MODIS aerosol data. We specifically focus upon fusing the CERES SSF with the MISR aerosol products. Although this project was undertaken specifically to address aerosol research, the methods employed for fusing data products can be used for other problems requiring synergistic data sets. We present selected case studies over different aerosol regimes and indicate that multisensor information provides value-added information for aerosol research that is not available from a single sensor.

Index Terms—Aerosol forcing, aerosols, climate, Clouds and the Earth’s Radiant Energy System (CERES), data fusion, Moderate Resolution Imaging Spectroradiometer (MODIS), Multi-angle Imaging SpectroRadiometer (MISR).

I. INTRODUCTION

ONE OF the major goals of the National Aeronautics and Space Administration (NASA)’s Earth Observing System (EOS) program is to study the Earth–atmosphere system in an integrated fashion [1]. As part of this vision, a series of individual and multisensor satellites was launched. The first EOS satellite, Terra, launched in December 1999, carried five sensors, including the Moderate Resolution Imaging Spectroradiometer (MODIS), the Multi-angle Imaging SpectroRadiometer (MISR), the Advanced Spaceborne Thermal Emission and Reflection Radiometer (ASTER), the Measurement of Pollution in the Troposphere (MOPITT) instrument, and the Clouds and the Earth’s Radiant Energy System (CERES). Since then, other satellites have been added, including: Aqua (in May 2002),

which was dedicated to studying the Earth’s water cycle; the Aura (in July 2004), for studying air quality and stratospheric ozone; the Polarization and Anisotropy of Reflectances for Atmospheric Science coupled with Observations from a Lidar (PARASOL), for studying clouds and aerosols; and the upcoming Orbiting Carbon Observatory (OCO) mission, for studying atmospheric carbon dioxide. In April 2006, the Cloud–Aerosol Lidar and Infrared Pathfinder Satellite Observation (CALIPSO) and CloudSat were also launched, and this combination of Aqua, Aura, PARASOL, OCO, CALIPSO, and CloudSat flying in formation within approximately 15 min of each other in a low orbit is called the A-Train, which will further enhance our research capabilities.

There is an increasing need to address scientific questions with combinations of data sets, utilizing the strengths of individual sensors and constraining weaknesses of others. These combined data sets can provide value-added information that would not be possible from one sensor only. In this paper, we discuss the concept of combining CERES, MODIS, and MISR (all aboard Terra) in the context of aerosol research.

CERES is a coarse spatial resolution (20 km² at nadir) broadband sensor that was designed to study top-of-the-atmosphere (TOA) fluxes. MODIS and MISR have higher resolutions (< 1 km), enabling better study of clouds and aerosols. MODIS has a larger horizontal swath, but MISR can address angular information [2]. MODIS and MISR data, averaged to CERES resolution, can help interpret CERES data as a function of clouds and aerosols. In fact, the CERES team has done merging of MODIS onto the CERES footprint, and this data set is called the CERES Single Scanner Footprint (SSF) product [3]. Level 1B MISR data have also been merged onto CERES SSF [4] but is not fully operational. In this paper, we combine both MODIS and MISR level 2 with CERES SSF data.

There are several data streams and products that are useful for atmospheric aerosol, cloud, and radiation budget research. In this paper, we focus primarily on examples related to the study of aerosols. The fundamental data product from satellite sensors are geo-referenced calibrated radiances at the sensors’ original resolution. These data are known as level 1B. Retrieved geophysical parameters are known as level 2 and are usually derived at predefined spatial resolutions (e.g., 10 km² for MODIS aerosol retrieval). Level 3 data are products provided on a regular latitude/longitude grid (e.g., 1 × 1° for MODIS aerosols). Each of these data is suited for different applications, ranging from image-based classification to validation/intercomparisons, to scientific applications such as the study of aerosol radiative forcing and assimilation into global climate models.

Several scientific questions related to air quality and radiative effects of aerosols, can be addressed using merged aerosol and

Manuscript received May 24, 2007; revised September 18, 2007. This work was supported in part by the National Aeronautics and Space Administration (NASA)’s Radiation Sciences, by Interdisciplinary Science, by an Earth Observing System grant, and by Atmospheric Chemistry Modeling and Analysis Programs. The work of P. Gupta was supported by NASA Headquarters under the Earth and Space Science Fellowship (NESSF) grant.

The authors are with the Department of Atmospheric Sciences, University of Alabama in Huntsville, Huntsville, AL 35899 USA (e-mail: sundar@nsstc.uah.edu).

Color versions of one or more of the figures in this paper are available online at <http://ieeexplore.ieee.org>.

Digital Object Identifier 10.1109/TGRS.2008.916087

93 radiation level 2 data products. Specifically, the combination of
94 MODIS, MISR, and CERES can help estimate aerosol radiative
95 effects. Until recently, MODIS aerosol products were not de-
96 rived over bright targets such as deserts. While the MODIS deep
97 blue algorithm [19], [20] now provides aerosol retrievals over
98 bright surfaces, it is not yet fully evaluated and has not yet been
99 fully processed for all Terra-MODIS data. MISR data, on the
100 other hand, have been validated over bright surfaces [5]. Since
101 MISR is limited in horizontal swath, as compared to MODIS,
102 but provides better retrievals in bright areas, it is desirable to
103 merge the two. While cross-sensor MODIS/MISR validation
104 [5] is not the focus of this paper, we use the MODIS and MISR
105 products together to estimate the aerosol properties for specific
106 cases (presented in Section IV).

107 It is generally believed that aerosols affect the climate sys-
108 tem significantly [6]. Since the launch of Terra and other
109 satellites, there is a shift from modeling-based assessments to
110 increasingly observational based approaches [7] for estimating
111 climate effects of aerosols. Another aspect of moving toward
112 an observational approach for studying aerosol radiative ef-
113 fects is the integration of energy budget (CERES) and imager
114 (MODIS/MISR) data sets from Terra [2], [8]. This method
115 provides an independent assessment of aerosol radiative effects,
116 which can be compared against modeling-based approaches.
117 While the CERES provides broadband TOA fluxes, multispec-
118 tral and multiangle measurements from MODIS and MISR
119 are needed to detect clouds and aerosols within the CERES
120 footprint and provide geophysical quantities such as aerosol
121 optical thickness (AOT) and particle size. Thus, combinations
122 of sensors can then be used to answer questions such as “What
123 is the radiative forcing of aerosols?” and “What is the radia-
124 tive forcing efficiency (aerosol forcing per unit optical depth),
125 and how does radiative forcing vary as a function of aerosol
126 properties?” The goal of this paper is to raise awareness of
127 multisensor data fusion to provide a framework for merging
128 level 2 aerosol data products at different spatial resolutions
129 and to finally provide some examples related to estimation of
130 aerosol radiative effects.

131 Data fusion can be defined as the merging of data from mul-
132 tiple sensors and related information from different databases
133 to achieve improved accuracy and more specific inferences [9].
134 Merging multiple satellite data sets utilizes the strengths of in-
135 dividual sensors, while constraining weaknesses of others. Past
136 research studies have successfully utilized merged satellite data
137 sets to assess landslide hazards using supervised classification
138 [12]. In the context of aerosol research, data fusion can be done
139 on different levels of data, such as radiance level 1B data [4],
140 geophysical parameters level 2 data (this paper), and gridded
141 level 3 data sets [10].

142 There are various issues related to data fusion, including
143 (but not limited to) data versions, error analysis of the indi-
144 vidual and the merged data products, and validation of these
145 products. For example, the CERES algorithm is processed at
146 NASA Langley with its own set of cloud and aerosol clearing
147 algorithms. MODIS aerosol product (MOD04) is generated at
148 the NASA Goddard Space Flight Center and then merged at
149 NASA Langley by the CERES science team called the CERES
150 SSF product. While the MODIS aerosol algorithm goes through

changes, and while newer versions are available (currently 151
collection 5), the CERES SSF product may not reflect the 152
MODIS product changes immediately due to data processing 153
timelines. The MISR level 2 data products that are developed 154
at the Jet Propulsion Laboratory are run routinely at NASA 155
Langley, although these products are not merged within the 156
CERES product routinely. Therefore, the best possible scenario 157
for independent users interested in data fusion is to obtain the 158
CERES SSF and merge the MISR aerosol products into the 159
CERES footprint, which is the focus of this paper. 160

161 II. DATA

In this section, we briefly describe the satellite sensors and 162
the data sets that are relevant to this paper. All of the data 163
sets are in hierarchical data format (hdf) and were obtained 164
through the NASA Langley Distributed Active Archive Center 165
(<http://eosweb.larc.nasa.gov>). The MODIS, MISR, and CERES 166
on Terra are in a polar-orbiting Sun-synchronous orbit at 167
705 km, with a descending equatorial crossing time of 168
10:30 A.M. The Terra satellite began collecting data in February 169
2000. Nearly 1 TB of global CERES, MODIS, and MISR data 170
were collected and processed for this research. 171

MODIS is a multispectral imaging radiometer that provide 172
measurements of the Earth’s land, ocean, and atmosphere with 173
36 spectral bands, covering the wavelength range from 0.405 to 174
14.385 μm with a swath width of 2330 km and providing global 175
coverage in 1–2 days [11]. The applicable MODIS data set in 176
this paper is the aerosol level 2 (collection 4) MOD04 products 177
at a 10-km² resolution, containing, among other parameters, the 178
AOT, the fine mode fraction, and the cloud fraction. A descrip- 179
tion of the MODIS aerosol retrieval algorithm and validation 180
strategies is fully explained in [12]. Table I shows some com- 181
monly used MODIS level 2 (MOD04) parameters for aerosol 182
research that are already merged within the CERES SSF files. 183

The MISR on Terra images the Earth in four spectral bands 184
(0.446, 0.557, 0.671, and 0.866 μm) and has nine push broom 185
cameras operating at nine different angles with a swath width 186
of about 360 km [13]. Due to the narrow swath width, near 187
global coverage is obtained only over 9 days at the equator and 188
2 days near the poles. There are 233 distinct repeating orbits 189
called paths, which are repeated every 16 days and are labeled 190
according to the Landsat Worldwide Reference System. To 191
simplify the processing and storing of these data over a large 192
geographical area, each MISR path is divided into a series 193
of predefined uniform-sized boxes along the ground track. 194
Each path is divided into 180 blocks, measuring 563.2 km 195
(cross-track) by 140.8 km (along-track). For a given path, a 196
numbered block always contains the same geographic location. 197

The relevant MISR data set for this paper is the level 2 198
aerosol data (MIL2ASAE), containing AOT at four spectral 199
channels, AOT values for three different size ranges of particles, 200
single-scattering albedo, and other related parameters (Table I). 201
These level 2 geophysical parameters are provided in a 202
17.6-km² spatial resolution. A detailed description of the 203
aerosol algorithm is given in [14]. Geographical information 204
on a Space Oblique Mercator (SOM) grid is given in the MISR 205
Ancillary Geographic Product (AGP). Geographical positions 206

TABLE I
SELECTED CERES SSF (INCLUDES MODIS AND CERES) AND MISR LEVEL 2 PARAMETERS COMMONLY USED IN AEROSOL RESEARCH

CERES SSF products	
1	CERES SW TOA flux
2	CERES LW TOA flux
3	CERES WN TOA flux
4	PSF-wtd MOD04 cloud fraction land
5	PSF-wtd MOD04 aerosol types land
6	PSF-wtd MOD04 corrected optical depth land (0.47, 0.55, 0.66)
7	PSF-wtd MOD04 cloud fraction ocean
8	PSF-wtd MOD04 effective optical depth average ocean (0.47, 0.55, 0.66, 0.86, 1.24, 1.64, 2.1)
9	PSF-wtd MOD04 optical depth small average ocean (0.55, 0.86, 2.1)
MISR level 2 aerosol products	
1	RegBestEstimateSpectralOptDepth (0.46, 0.55, 0.67, 0.86)
2	RegBestEstimateAngstromExponent
3	RegBestEstimateSpectralSSA (0.46, 0.55, 0.67, 0.86)
4	RegBestEstimateSpectralOptDepthFraction
5	RegBestEstimateNumberFraction
6	RegBestEstimateVolumeFraction

207 of MISR pixels in terms of latitude and longitude are provided
208 in a 1.1-km² grid resolution and stored in separate files for
209 each fixed MISR orbit. These 233 files corresponding to 233
210 distinct MISR orbits provided as separate parameters can be
211 used to geolocate the level 2 data products (Table I).

212 The CERES provides broadband radiative energy measure-
213 ments at the TOA, both in the long and short waves [15]. Each
214 CERES instrument has three channels: 1) a short-wave channel
215 for measuring reflected sunlight (0.3–5 μm); 2) a long-wave
216 channel for measuring Earth-emitted thermal radiation in the
217 8–12- μm “window” region; and 3) a total channel for radiation
218 between 0.3 and 200 μm . The Terra carries two identical
219 CERES instruments: one operates in a cross-track scan mode
220 (FM-1) and the other in a biaxial scan mode (FM-2) for
221 developing angular models to convert the measured broadband
222 radiances to fluxes. On Terra, the CERES has a spatial resolu-
223 tion of approximately 20 km² (equivalent diameter) at nadir.

224 For each CERES footprint, the MODIS AOT and other
225 relevant aerosol information from MODIS are convolved using
226 point spread functions (PSFs) and matched in space and time to
227 the CERES measurement [16] and are available as the CERES
228 SSF product. Therefore, for each CERES footprint, the PSF-
229 weighted cloud fraction and aerosol properties such as optical
230 depth are provided only from the MODIS data. The CERES
231 SSF data can be ordered online for user-selected regions and
232 parameters of interest. There are 160 parameters for each pixel,
233 ranging from geolocation information, Sun–satellite geometry,
234 cloud and aerosol information, and CERES radiative energy
235 fluxes (Table I).

236 For illustrative purposes, Fig. 1 shows an example of an
237 aerosol event observed by the three different sensors from Terra
238 on October 26, 2003. Fig. 1(a) shows a true-color composite
239 of channel 0.67 μm in red, channel 0.55 μm in green, and
240 channel 0.47 μm in blue around the west coast of the U.S.
241 from the MODIS level 1B data. Fig. 1(b) shows the MISR
242 (version F03, V002 data) data for the same day using similar
243 bands as MODIS. Both MODIS and MISR clearly show the
244 large smoke plumes from the west coast of California. The
245 CERES short-wave flux is shown in Fig. 1(c) from this period,
246 and the image appears blocky when compared to the MODIS

and MISR imagery due to the large pixel size of the CERES
247 scanner. Note the large swath width of the MODIS and CERES
248 when compared to the MISR. Dark areas correspond to ocean
249 background, whereas smoke plumes from the fires and the
250 clouds appear brighter due to higher reflectivity when compared
251 to the background. This difference in contrast between the
252 background and aerosols is used to separate aerosols and clouds
253 and is further used to retrieve aerosol properties by the MODIS
254 and MISR algorithms. The corresponding level 2 MODIS and
255 MISR (version F09, V002) AOT images are shown in Fig. 2(a)
256 and (b), respectively. MODIS uses multispectral methods, state-
257 of-the-art cloud clearing techniques, and predefined aerosol
258 models to retrieve the AOT value at 10 km² [12]. On the other
259 hand, MISR uses multispectral multiangle information and pre-
260 defined aerosol models to provide AOT retrievals over 17.6 km²
261 [14]. Both algorithms continue to undergo developments and
262 refinements with intensive validation against ground and
263 suborbital measurements. The CERES can be used directly to
264 obtain TOA short-wave fluxes due to smoke aerosols, provided
265 the aerosols can be identified using MODIS and MISR data.
266 This multisensor combination is powerful for studying aerosol
267 radiative effects from an observational perspective [2]. 268

III. METHODOLOGY

269

270 One of the goals of this paper is to demonstrate fusion of
271 CERES SSF and MISR level 2 aerosol products and show some
272 selected examples related to aerosol research. To merge MISR
273 level 2 aerosol (MIL2ASAE) products with CERES SSF (FM1,
274 Edition2B) in space and time, a collocation algorithm is first
275 developed. Since the three sensors are all on the same satellite,
276 collocation by time is simple.

277 A simple flowchart of the algorithm is shown in Fig. 3,
278 and since handling MISR data sets is not straightforward, the
279 methodology is described in detail. Each CERES SSF file
280 includes all geophysical parameters (such as TOA short- and
281 long-wave fluxes), geolocation information, and Sun–satellite
282 geometry, along with MODIS spectral AOTs and the MODIS
283 cloud fraction within each CERES footprint. There are about
284 160 parameters in the CERES SSF file, and any of these

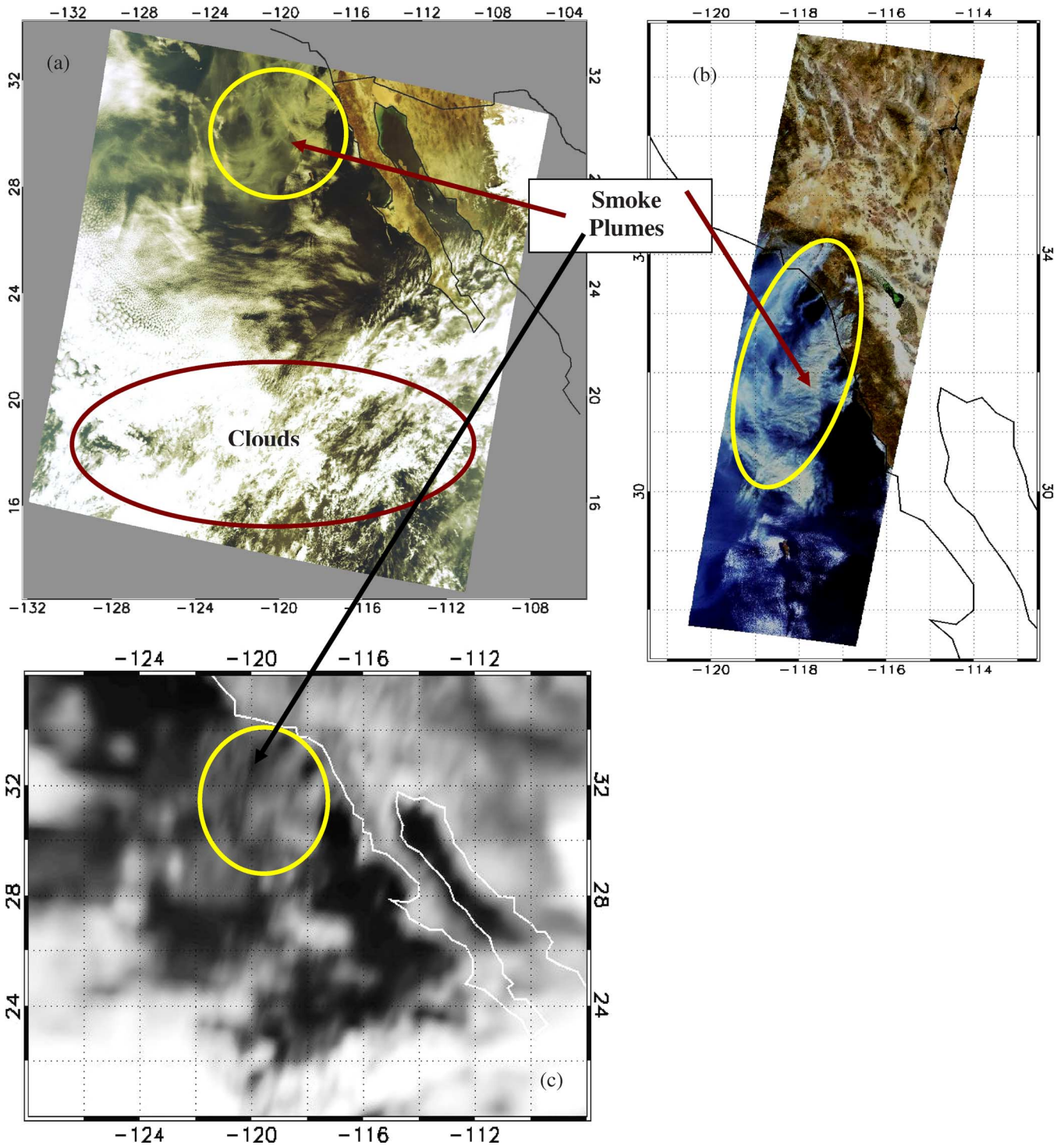


Fig. 1. True-color image of biomass burning event in the western U.S. on October 26, 2003, at 1840 GMT from (a) Terra-MODIS, (b) MISR nadir view, and (c) CERES short-wave flux.

285 parameters in combination with the MISR products can be
 286 obtained from our general-purpose software. The CERES
 287 SSF files contain data for a 1-h observation period, and
 288 date-time information is part of the filename. A typical
 289 CERES SSF file is named CER_SSF_Terra-FM1-MODIS_
 290 Edition2B_YYYYMMDDHH.hdf from the Terra satellite
 291 where CER indicates CERES, FM1 denotes that the data are
 292 from the cross-track scanner, and YYYY, MM, DD, and HH
 293 are the year, month, day, and hour, respectively.

The MISR products do not contain geolocation information
 294 such as latitude and longitude in the same file. However, the
 295 new data ordering tools provide some options to the user to add
 296 this information in the data file. The geolocation information
 297 is fixed for the 233 predefined MISR orbits and is available as
 298 separate files. The typical file naming of the geolocation file
 299 is MISR_AM1_AGP_Pathnumber_F01_24.hdf. Similar to the
 300 CERES SSF, the MISR data files contain many parameters,
 301 including spectral AOT, single-scattering albedo, Angstrom
 302

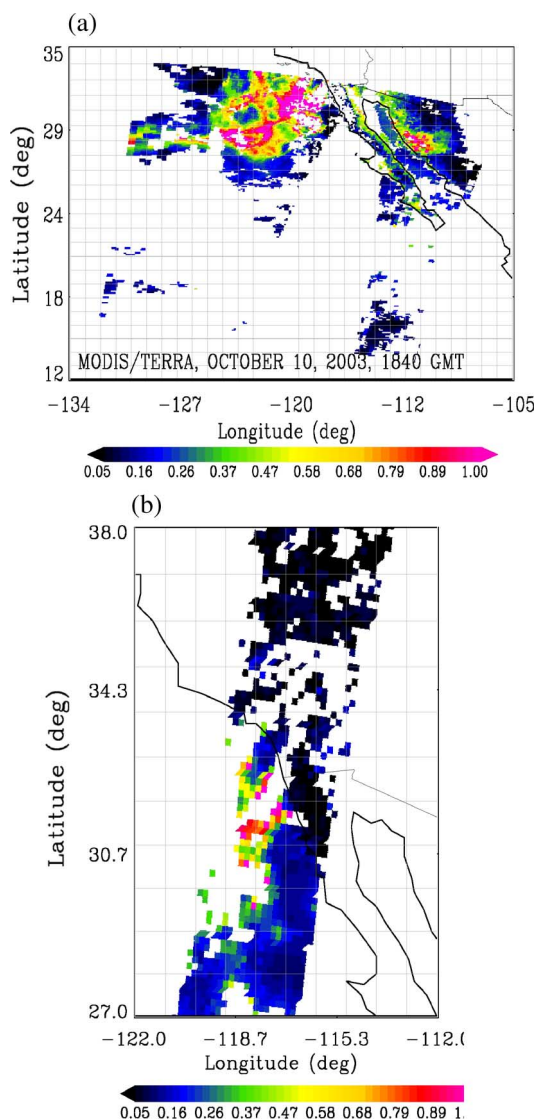


Fig. 2. Midvisible AOT from level 2 aerosol products from (a) MODIS and (b) MISR for the images shown in Fig. 1. Missing values in AOT are due to clouds.

303 coefficient, and size-fractioned AOTs. A total of 121 parameters
 304 are available from the MISR aerosol product, and our software
 305 is flexible enough to accommodate any combination of these
 306 parameters to be collocated with CERES SSF in space and time.
 307 Although each MISR path contains 180 blocks, due to seasonal
 308 variations in the portion of the Earth that is in daylight, only
 309 up to 142 blocks contain valid data points. Valid MISR aerosol
 310 retrieval blocks are identified using start and end block numbers
 311 provided in the data file. Then, the date and time parameters
 312 are obtained for the same blocks. The MISR does not provide
 313 date and time for each pixel, but it provides information for
 314 the center of each block. Interpolation is performed to obtain
 315 the time information for each pixel within a given block. MISR
 316 latitude and longitude data are in a 1.1-km² resolution, whereas
 317 MISR aerosol products are in a 17.6-km² resolution. For each
 318 valid data pixel, the corresponding latitude and longitude is
 319 obtained by selecting the center latitude and longitude of the
 320 box of 16 × 16 pixels in geolocation data.

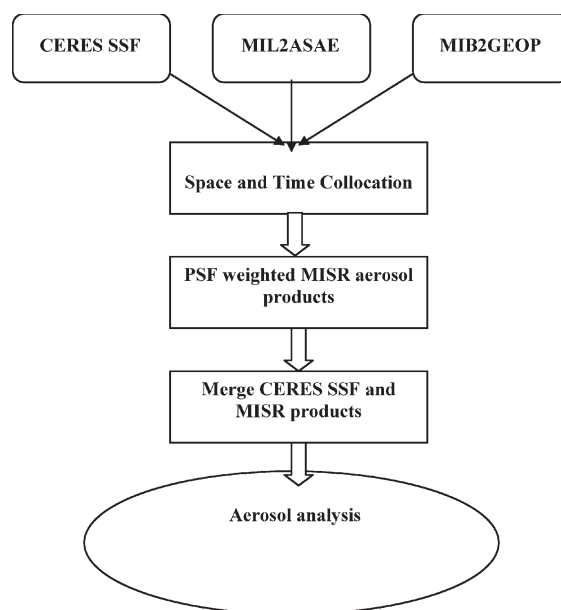


Fig. 3. Flowchart of the space and time collocation between the CERES SSF and MISR level 2 products. The CERES SSF product contains the CERES and merged MODIS data, and MIL2ASAE and MIB2GEOP are the MISR aerosol product data set and the geolocation files, respectively.

The main collocation algorithm is divided into two sections. The first section deals with collocation in time, whereas the second deals with collocation in space. Since both the CERES and the MISR are onboard Terra, they provide near-simultaneous observations. The key issue in time collocation is how to find the appropriate MISR file corresponding to the CERES observation period, and this is done by checking both day and time information. Since the MISR filename does not have date–time information, this becomes a cumbersome process. To increase searching efficiency, a separate database of date and time corresponding to the various orbits and path numbers are used to select the proper file corresponding to each CERES file. On proper selection of MISR file, the CERES SSF observation date and time information is matched with the MISR date/time, and then, the collocation in space begins. Since the sensors are on the same satellite, the observation time is almost the same, and therefore, temporal collocation is not necessary. To make the computer code more efficient and useful to the users, spatial collocation is performed only over the user-selected area of interest, which can be input to the algorithm by providing the latitude and longitude of the four corners of a region. Since the CERES and MISR have different ground resolutions, exact or one-to-one collocation in space may not be possible. Another important thing to note is the CERES pixel size, which can be larger than 100 km² at the edge of the CERES swath due to panoramic distortion, is an important factor when collocating MODIS and CERES. However, since the MISR swath is narrow, and it is in the middle of the CERES swath, panoramic distortion in the MISR is not significant.

The CERES pixel shape and size is not fixed, and it is therefore difficult to define its size parameters. Our algorithm uses two different averaging methods: one is simple arithmetic-weighted average, and the other one uses the CERES PSF average. In the first method, the CERES pixel is assumed to be

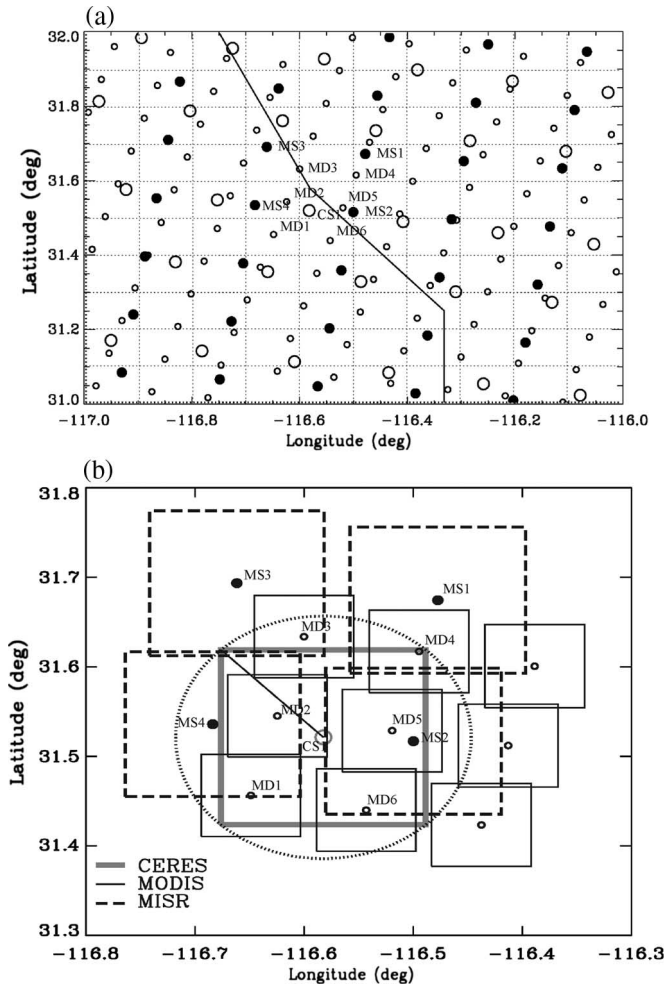


Fig. 4. (a) Latitude and longitude of MISR, MODIS, and CERES pixels for a small portion of the swath and (b) the collocation of one CERES pixel with multiple MISR pixels. The location of the CERES pixel is shown by a large unfilled circle, MODIS by a small unfilled circle, and MISR pixel by a medium unfilled circle. The CERES pixel CS1 in (a) is shown in greater detail in (b). The MODIS pixels are labeled MD, and the MISR pixels are labeled MS.

355 rectangular with one edge as defined by along-track dimension
 356 and with the other edge as defined by across-track length,
 357 although other shape functions can easily be accommodated.
 358 The second method uses PSF to map the MISR data to the
 359 CERES pixel. Fig. 4(a) shows a small section of the MODIS,
 360 MISR, and CERES swath, indicating the relative size of each
 361 pixel, as well as the collocation procedure. Both along- and
 362 across-track lengths for each rectangular pixel are calculated
 363 using viewing zenith angle information, and correction due
 364 to the Earth's curvature is also made. Fig. 4(b) shows the
 365 collocation procedure for one CERES pixel (CS1) and the
 366 corresponding MODIS (MD) and MISR (MS) pixels. The size
 367 of each MODIS, MISR, and CERES pixel is indicated and is
 368 approximately equal to the dimensions at nadir [Fig. 4(b)]. The
 369 circle denotes the search radius used in calculating mean MISR
 370 values from all the pixels falling within the CS1 pixel.

371 To obtain the MISR product value at CERES pixel location
 372 and resolution, the spherical distance that accounts for the
 373 curvature of the Earth between the MISR and CERES pixel is
 374 calculated. All the MISR pixels falling within the circle with
 375 the radius that is half of the diagonal of the CERES pixel are

averaged using two different methods. The first method uses the 376
 arithmetic average of all MISR parameters (e.g., AOT) falling 377
 within the circle. The second uses the distance weighted aver- 378
 age, where all the MISR pixels falling within the CERES circle 379
 receive a weight between 0 and 1 based on how close it is from 380
 the center of the CERES pixel. There are numerous weighting 381
 function options that are available, and we used the inverse 382
 distance weighting, where weights are a decreasing function of 383
 distance. The third option (second averaging approach) used is 384
 the CERES PSF weighted average [17] value of MISR AOT 385
 at the CERES footprint. The CERES convolution algorithm 386
 weights the MISR pixel based on where it is located within the 387
 CERES pixel [4]. 388

IV. APPLICATION OF MERGED MODIS-MISR-CERES DATASETS 389 390

We provide three selected examples of the collocated aerosol 391
 and flux data from MODIS, MISR, and CERES over three 392
 different regimes [Fig. 5(a)–(e)]. Also included in one case 393
 study is the comparison of the MISR AOT with ground-based 394
 sunphotometer values. 395

A. MISR, MODIS, and AERONET AOT 396

Fig. 5(a) shows the level 2 AOT from the MODIS and 397
 MISR over the Sahara Desert for January 16, 2006. Two whole 398
 MODIS swaths and a partial swath show the large MODIS 399
 coverage over this area. Note that the MODIS AOT retrievals 400
 are only available over cloud-free vegetated surfaces (dark 401
 target) and, therefore, are restricted to latitudes between 0° N 402
 and 15° N in the area of study, and no retrievals are available 403
 in the desert regions shown in gray color. The MISR, on the 404
 other hand, has three narrow swaths during this day but has 405
 complete aerosol retrievals over all surface types, except in 406
 cloudy conditions that can be used to fill in AOT values where 407
 MODIS retrievals are not available. Also shown in black dots 408
 are several Aerosol Robotic Network (AERONET) locations 409
 that are currently the standard for validating aerosol retrievals. 410
 Comparisons between satellite retrievals and AERONET loca- 411
 tions are important for testing the robustness of the satellite 412
 retrievals. An intercomparison of the MISR 17.6-km² AOT 413
 retrievals with ± 30 min of AOT values from AERONET is 414
 shown in Fig. 5(b). This intercomparison is performed on all the 415
 AERONET stations shown in Fig. 5(a) during January to March 416
 2006. An excellent correlation between the two retrievals indi- 417
 cates the high quality of the MISR retrievals over bright targets 418
 such as deserts and is especially useful in these areas where 419
 MODIS retrievals are not possible. 420

B. Use of MODIS, MISR, and CERES for Estimating LWRE 421

Including MISR into the CERES SSF product will enable 422
 us to estimate TOA long-wave radiative effect (LWRE) as a 423
 function of aerosol properties even over bright surfaces. The 424
 LWRE is defined as the difference in CERES TOA long-wave 425
 fluxes with and without the presence of aerosols. Fig. 5(c), 426
 which was adapted from [2], shows the spatial distribution of 427
 MISR AOT for September 2000 over the Sahara Desert [2]. In 428

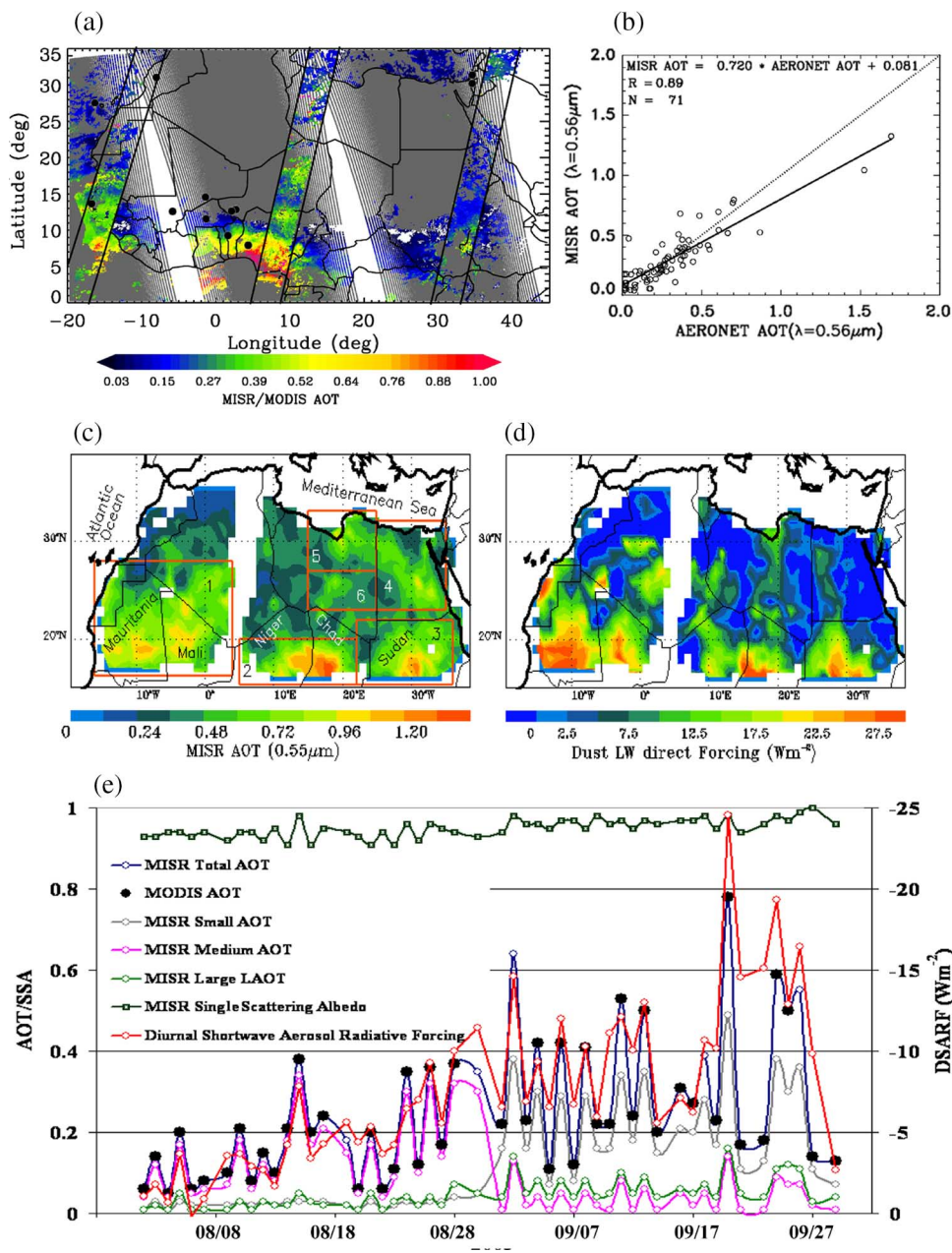


Fig. 5. Case studies of data fusion. (a) Spatial distribution of MISR and MODIS derived AOT on January 16, 2006 over North Africa. (b) MISR AOT versus AERONET AOT. (c) MISR AOT for September 2004. (d) CERES-derived long-wave dust aerosol radiative effect (from [2]). (e) Time series of MODIS- and MISR-derived aerosol properties, along with the CERES biomass burning aerosol effect over the Amazon basin during August and September 2003.

429 the Sahara Desert regions, MODIS retrievals were not available,
 430 and therefore, the MISR AOT values were used in conjunction
 431 with the CERES data for addressing dust radiative effects.
 432 MODIS cloud information was used to remove cloud contam-
 433 ination within the CERES pixel since the MODIS offers more
 434 channels and a higher spatial resolution to detect clouds. During
 435 this month, closer to the equator, biomass burning activities are
 436 responsible for the high AOT observed in this region. Away
 437 from the equator, dust aerosols increase the AOT, and several re-
 438 gions labeled 1–6 in Fig. 5(c) indicate the high AOT that MISR
 439 retrieves. The collocated MODIS–MISR–CERES data sets can
 440 then be used to address the effects of dust aerosols on the radia-
 441 tive balance of the Earth–atmosphere system. Fig. 5(d) shows
 442 the long-wave TOA dust aerosol radiative forcing. Positive

aerosol LWRE values indicate that the aerosols emit at a colder
 443 temperature when compared to the Earth’s surface, thereby
 444 reducing the amount of Earth-emitted radiation back to space,
 445 thereby creating a “warming effect” that is opposite in effect
 446 to that of the short-wave reflective nature of other aerosols [2].
 447 This example clearly shows the potential of using MODIS and
 448 MISR aerosol properties over bright targets along with CERES
 449 observations, which is not possible by using one sensor alone. 450

C. Use of MODIS, MISR, and CERES for Studying Biomass Burning Aerosols 451
 452

We move from a highly reflective background in Africa, 453
 where dust is prevalent, to another example over South 454

455 America, where the reflectivity is low and where biomass burn-
 456 ing aerosols are prevalent. In South America, each year during
 457 the dry season, agricultural activities result in several teragrams
 458 of smoke aerosols that are released into the atmosphere. These
 459 aerosols affect the regional radiative balance significantly.
 460 MODIS and MISR can be used to map the spatial distribution of
 461 aerosols. Retrieved AOT and aerosol properties from MISR can
 462 be used to further study aerosol forcing as a function of various
 463 aerosol properties. Fig. 5(e) presents the time series of aerosol
 464 properties from MISR and short-wave forcing over the Amazon
 465 basin (20° S–0° N and 65° S–45° S) during August and
 466 September 2003 estimated using merged MODIS–MISR–
 467 CERES data sets. Again, cloud clearing of CERES pixels has
 468 been done using MODIS data. MISR retrieval produces aerosol
 469 parameters, including the AOT due to small-, medium-, and
 470 large-sized particles, as well as the total AOT at 0.55 μm ,
 471 along with single-scattering albedo and Angstrom coefficient.
 472 The short-wave forcing is the difference in the TOA short-wave
 473 flux between clear and aerosol regions, which is an important
 474 parameter for climate research.

475 This time series shows diurnally averaged short-wave aerosol
 476 radiative forcing (DSARF) and the associated aerosol proper-
 477 ties. The DSARF is defined as the difference between clear-
 478 sky (F_{clr}) and aerosol-sky fluxes (F_{aero}) that is adjusted for
 479 diurnal effects [22]. F_{clr} corresponds to cloud- and aerosol-
 480 free fluxes, while F_{aero} corresponds to cloud-free fluxes from
 481 regions where aerosols are present [2]. Here, it is important
 482 to note that during August and September, the study region in
 483 South America is dominated by anthropogenic biomass burning
 484 aerosols, and hence, the term “radiative forcing” is used instead
 485 of “radiative effects” [7].

486 Fig. 5(e) clearly shows that both AOT and DSARF increases
 487 from August to September, which was mainly due to the
 488 increase in biomass burning activities in the region. Also, the
 489 AOTs due to medium-sized particles contribute more in total
 490 AOT during August, but small mode contribution is more in
 491 September compared to any other size mode. For comparison,
 492 the MODIS total AOT is shown as black dots, and it compares
 493 remarkably well with the MISR total AOT shown in blue over
 494 this region. Further analysis is provided in Patadia *et al.* [18]
 495 who quantitatively discuss what portion of the AOT and forcing
 496 comes from various particle sizes. Collocated data sets such as
 497 these can be used to further improve our understanding of the
 498 role of aerosols on the energy balance of the Earth–atmosphere
 499 system.

500

V. SUMMARY

501 There are many satellite sensors that are currently in orbit
 502 for studying the Earth–atmosphere in an integrated fashion.
 503 However, most studies to date largely focus upon single-sensor
 504 approaches for studying specific problems. This is largely
 505 due to the complexities in merging data and the volume of
 506 data involved. There are various methods for merging data at
 507 different processing levels. While some applications require
 508 merging of radiance level data (level 1), this could often be
 509 time consuming and laborious. However, there are a variety
 510 of retrieved products (level 2) at different spatial and temporal

resolutions that could be merged to address scientific issues. 511
 While the ideal scenario is to have a unified cloud-clearing 512
 algorithm across all sensors and then retrieve aerosol properties 513
 and convolve it within the CERES footprint, this is not the 514
 current practice. Therefore, some of the product level data 515
 fusion has to be done by individual researchers. 516

In this paper, we have combined three data sets, namely, 517
 the MODIS, the MISR, and the CERES for studying common 518
 problems in aerosol research. Note that the MODIS and CERES 519
 have already been merged at NASA Langley (the CERES SSF 520
 product). We merge the level 2 MISR aerosol product with 521
 the CERES SSF data. Each data set has numerous retrieved 522
 parameters and different algorithms for creating these param- 523
 eters. We have not attempted to discuss the algorithms, the 524
 retrievals, or the accuracies since they are not the focus of 525
 this paper. Our major goal has been to raise the awareness of 526
 multisensor data fusion from sensors on a single satellite and 527
 provide a simple framework for merging data. In the process, 528
 we have also provided some selected examples. These are not 529
 meant to be exhaustive by any means. However, our examples 530
 indicate the robustness of the data fusion methods and value- 531
 added information, since the geophysical parameters such as 532
 AOT and short- and long-wave forcing are consistent with other 533
 research studies. We now have software in place that can be 534
 used to merge these types of data sets for aerosol and possibly 535
 cloud research. With the series of satellites as part of the 536
 A-train that will obtain data over a pixel within seconds to 537
 several minutes of each other, collocation issues could be 538
 challenging, and further research is necessary to merge data 539
 from multiple satellites for addressing research questions. 540

ACKNOWLEDGMENT

The authors would like to thank the Atmospheric Sciences 542
 Data Center at the NASA Langley Research Center, from which 543
 the data were obtained. 544

REFERENCES

- [1] G. Asrar and J. Dozier, *EOS: Science Strategy for the Earth Observing* 546
System. New York: AIP, 1994. 547
- [2] J. Zhang and S. A. Christopher, “Longwave radiative forcing of dust 548
 aerosols over the Saharan Desert estimated from MODIS, MISR, and 549
 CERES observations from Terra.” *Geophys. Res. Lett.*, vol. 30, no. 23, 550
 2188, 2003. DOI: 10.1029/2003GL018479. 551
- [3] E. B. Geier, R. N. Green, D. P. Kratz, P. Minnis, W. F. Miller, 552
 S. K. Nolan, and C. B. Franklin, *Single Satellite Footprint TOA/Surface* 553
Fluxes And Clouds (SSF) Collection Document. Hampton, VA: NASA 554
 Langley Res. Center, 2001. [Online]. Available: [http://asd-www.larc.](http://asd-www.larc.nasa.gov/ceres/collect_guide/SSF_CG.pdf) 555
[nasa.gov/ceres/collect_guide/SSF_CG.pdf](http://asd-www.larc.nasa.gov/ceres/collect_guide/SSF_CG.pdf) 556
- [4] N. G. Loeb, W. Sun, W. F. Miller, K. Loukachine, and R. Davies, “Fu- 557
 sion of CERES, MISR, and MODIS measurements for top-of-atmosphere 558
 radiative flux validation,” *J. Geophys. Res.*, vol. 111, no. D18, D18209, 559
 2006. DOI: 10.1029/2006JD007146. 560
- [5] W. A. Abdou, D. J. Diner, J. V. Martonchik, C. J. Bruegge, R. A. Kahn, 561
 B. J. Gaitley, K. A. Crean, L. A. Remer, and B. Holben, “Compari- 562
 son of coincident Multiangle Imaging Spectroradiometer and Moderate 563
 Resolution Imaging Spectroradiometer aerosol optical depths over land 564
 and ocean scenes containing aerosol robotic network sites,” *J. Geophys.* 565
Res.—Atmos., vol. 110, no. D10, pp. 11 967–11 976, 2005. D10S07. 566
- [6] M. Bellouin, O. Boucher, J. Haywood, and M. S. Reddy, “Global estimate 567
 of aerosol direct radiative forcing from satellite measurements,” *Nature*, 568
 vol. 438, no. 7071, pp. 1138–1141, Dec. 2005. 569
- [7] T. L. Anderson, R. J. Charlson, N. Bellouin, O. Boucher, M. Chin, 570
 S. A. Christopher, H. J. Haywood, Y. J. Kaufman, S. Kinne, J. Ogren, 571

- 572 L. A. Remer, T. Takemura, D. Tanre, O. Torres, C. R. Trepte,
573 B. A. Wielicki, D. Winker, and H. Yu, "An A-Train strategy for quan-
574 tifying direct climate forcing by anthropogenic aerosols," *Bull. Amer.*
575 *Meteorol. Soc.*, vol. 86, no. 12, pp. 1795–1809, 2005.
- 576 [8] S. A. Christopher and J. Zhang, "Cloud-free shortwave aerosol radiative
577 effect over oceans: Strategies for identifying anthropogenic forcing
578 from Terra satellite measurements," *Geophys. Res. Lett.*, vol. 31, no. 18,
579 L18 101, 2004. DOI: 10.1029/2004GL020510.
- 580 [9] L. Wald, "Some terms of reference in data fusion," *IEEE Trans. Geosci.*
581 *Remote Sens.*, vol. 37, no. 3, pp. 1190–1193, May 1999.
- 582 [10] J. Acker and G. Leptoukh, "Online analysis enhances use of NASA Earth
583 science data," *Eos Trans. AGU*, vol. 88, no. 2, pp. 14–17, 2007.
- 584 [11] P. E. Ardanuy, D. Han, and V. V. Salomonson, "The Moderate Resolution
585 Imaging Spectrometer (MODIS) science and data system requirements,"
586 *IEEE Trans. Geosci. Remote Sens.*, vol. 29, no. 1, pp. 75–88, Jan. 1991.
- 587 [12] L. A. Remer, Y. J. Kaufman, D. Tanré, S. Mattoo, D. A. Chu, J. V. Martins,
588 R.-R. Li, C. Ichoku, R. C. Levy, R. G. Kleidman, T. F. Eck,
589 E. Vermote, and B. N. Holben, "The MODIS aerosol algorithm, products
590 and validation," *J. Atmos. Sci.*, vol. 62, no. 4, pp. 947–973, Apr. 2005.
- 591 [13] D. J. Diner, J. C. Beckert, G. W. Bothwell, and J. I. Rodriguez, "Per-
592 formance of the MISR instrument during its first 20 months in Earth
593 orbit," *IEEE Trans. Geosci. Remote Sens.*, vol. 40, no. 7, pp. 1449–1466,
594 Jul. 2002.
- 595 [14] R. Kahn, B. Gaitley, J. Martonchik, D. Diner, K. Crean, and B. Holben,
596 "Multiangle Imaging Spectroradiometer (MISR) global aerosol optical
597 depth validation based on two years of coincident AERONET observa-
598 tions," *J. Geophys. Res.—Atmos.*, vol. 110, no. D10, D10S04, 2005. DOI:
599 j0004706R.
- 600 [15] B. A. Wielicki, B. R. Barkstrom, E. F. Harrison, R. B. Lee, III,
601 G. L. Smith, and J. E. Cooper, "Clouds and the Earth's radiant energy
602 system (CERES): An Earth Observing System experiment," *Bull. Amer.*
603 *Meteorol. Soc.*, vol. 77, no. 5, pp. 853–868, May 1996.
- 604 [16] G. L. Smith, "Effects of time response on the point spread function
605 of a scanning radiometer," *Appl. Opt.*, vol. 33, no. 30, pp. 7031–7037,
606 Oct. 1994.
- 607 [17] R. N. Green and B. A. Wielicki, *Convolution of Imager Cloud Prop-*
608 *erties With CERES Footprint Point Spread Function (Subsystem 4. 4),*
609 *Clouds and the Earth's Radiant Energy System (CERES) Algorithm*
610 *Theoretical Basis Document*. Hampton, VA: NASA Langley Res.
611 Center, 1996. [Online]. Available: <http://asd-www.larc.nasa.gov/ATBD/ATBD.html>
- 612
- 613 [18] F. Patadia, P. Gupta, S. A. Christopher, and J. S. Reid, "A multi-year data
614 fusion approach for assessing biomass burning aerosol radiative impacts
615 over Amazonia," *J. Geophys. Res.*, 2008. DOI:10.1029/2007JD009486.
- 616 [19] N. C. Hsu, S. C. Tsay, M. D. King, and J. R. Herman, "Aerosol properties
617 over bright-reflecting source regions," *IEEE Trans. Geosci. Remote Sens.*,
618 vol. 42, no. 3, pp. 557–569, Mar. 2004.
- 619 [20] N. C. Hsu, S. C. Tsay, M. D. King, and J. R. Herman, "Deep blue
620 retrievals of Asian aerosol properties during ACE-Asia," *IEEE Trans.*
621 *Geosci. Remote Sens.*, vol. 44, no. 11, pp. 3180–3195, Nov. 2006.
- 622 [21] Y.-L. Chang, L.-S. Liang, C.-C. Han, J.-P. Fang, W.-Y. Liang, and
623 K.-S. Chen, "Multisource data fusion for landslide classification using
624 generalized positive Boolean functions," *IEEE Trans. Geosci. Remote*
625 *Sens.*, vol. 45, no. 6, pp. 1697–1708, Jun. 2007.
- 626 [22] L. A. Remer and Y. J. Kaufman, "Aerosol effect on the distribution of
627 solar radiation over the clear-sky global oceans derived from four years of
628 MODIS retrievals," *Atmos. Chem. Phys. Discuss.*, vol. 5, no. 4, pp. 5007–
629 5038, 2005.



Pawan Gupta received the M.Sc. degree in physics 630
from Devi Ahilya University, Indore, India, in 631
2000 and the M.Tech. degree in space and at- 632
mospheric sciences from the Physical Research Lab- 633
oratory, Ahmedabad, India, and Andhra University, 634
Visakhapatnam, India, in 2003. He is currently work- 635
ing toward the Ph.D. degree in atmospheric science 636
at the University of Alabama, Huntsville. 637

From 2002 to 2003, he was a Junior Research 638
Fellow at the National Remote Sensing Agency, 639
Hyderabad, India. In 2005, he received NASA's 640

Graduate Student Fellowship in Earth Systems Science. His current research 641
interests mainly include the study of atmospheric aerosols, satellite remote 642
sensing of aerosols and particulate matter air quality, Earth-atmosphere ra- 643
diation budget, and data fusion from multiple satellite and surface based 644
instruments. 645



Falguni Patadia received the M.Sc. degree in 646
physics from Devi Ahilya University, Indore, 647
India, in 2000 and the M.Tech. degree in space and 648
atmospheric sciences from the Physical Research 649
Laboratory, Ahmedabad, India, and Andhra Univer- 650
sity, Visakhapatnam, India, in 2003. She is currently 651
working toward the Ph.D. degree in atmospheric 652
science at the University of Alabama in Huntsville. 653

Her current research interests mainly include the 654
study of atmospheric aerosols, satellite remote sens- 655
ing of aerosols, and data fusion of multiple satellite 656

and surface-based measurements for studying the role of tropospheric aerosols 657
on Earth's radiation budget. 658



Sundar A. Christopher received the Ph.D. degree 659
in atmospheric sciences from Colorado State Uni- 660
versity, Fort Collins, in 1995. He received the M.S. 661
degree in meteorology from the South Dakota School 662
of Mines and Technology, Rapid City, and the M.S. 663
degree in industrial/organizational psychology from 664
the University of Alabama, Huntsville (UAH). 665

He is currently a Professor in the Department of 666
Atmospheric Sciences and the Associate Director 667
of the Earth System Science Center at UAH. His 668
research interests include satellite remote sensing of 669

clouds and aerosols and their impact on air quality and global and regional 670
climate. 671

Multisensor Data Product Fusion for Aerosol Research

Pawan Gupta, Falguni Patadia, and Sundar A. Christopher

Abstract—Combining data sets from multiple satellite sensors is a powerful method for studying Earth–atmosphere problems. By fusing data, we can utilize the strengths of the individual sensors that may not be otherwise possible. In this paper, we provide the framework for combining level 2 data products, using data from three sensors aboard the National Aeronautics and Space Administration (NASA)’s Terra satellite. These data include top-of-the-atmosphere (TOA) radiative energy fluxes obtained from the Clouds and the Earth’s Radiant Energy System (CERES), aerosol optical thickness from the multispectral Moderate Resolution Imaging Spectroradiometer (MODIS), and aerosol properties from the Multi-angle Imaging SpectroRadiometer (MISR). The CERES Single Scanner Footprint (SSF) contains the pixel level CERES TOA fluxes and the level 2 MODIS aerosol data. We specifically focus upon fusing the CERES SSF with the MISR aerosol products. Although this project was undertaken specifically to address aerosol research, the methods employed for fusing data products can be used for other problems requiring synergistic data sets. We present selected case studies over different aerosol regimes and indicate that multisensor information provides value-added information for aerosol research that is not available from a single sensor.

Index Terms—Aerosol forcing, aerosols, climate, Clouds and the Earth’s Radiant Energy System (CERES), data fusion, Moderate Resolution Imaging Spectroradiometer (MODIS), Multi-angle Imaging SpectroRadiometer (MISR).

I. INTRODUCTION

ONE OF the major goals of the National Aeronautics and Space Administration (NASA)’s Earth Observing System (EOS) program is to study the Earth–atmosphere system in an integrated fashion [1]. As part of this vision, a series of individual and multisensor satellites was launched. The first EOS satellite, Terra, launched in December 1999, carried five sensors, including the Moderate Resolution Imaging Spectroradiometer (MODIS), the Multi-angle Imaging SpectroRadiometer (MISR), the Advanced Spaceborne Thermal Emission and Reflection Radiometer (ASTER), the Measurement of Pollution in the Troposphere (MOPITT) instrument, and the Clouds and the Earth’s Radiant Energy System (CERES). Since then, other satellites have been added, including: Aqua (in May 2002),

which was dedicated to studying the Earth’s water cycle; the Aura (in July 2004), for studying air quality and stratospheric ozone; the Polarization and Anisotropy of Reflectances for Atmospheric Science coupled with Observations from a Lidar (PARASOL), for studying clouds and aerosols; and the upcoming Orbiting Carbon Observatory (OCO) mission, for studying atmospheric carbon dioxide. In April 2006, the Cloud–Aerosol Lidar and Infrared Pathfinder Satellite Observation (CALIPSO) and CloudSat were also launched, and this combination of Aqua, Aura, PARASOL, OCO, CALIPSO, and CloudSat flying in formation within approximately 15 min of each other in a low orbit is called the A-Train, which will further enhance our research capabilities.

There is an increasing need to address scientific questions with combinations of data sets, utilizing the strengths of individual sensors and constraining weaknesses of others. These combined data sets can provide value-added information that would not be possible from one sensor only. In this paper, we discuss the concept of combining CERES, MODIS, and MISR (all aboard Terra) in the context of aerosol research.

CERES is a coarse spatial resolution (20 km² at nadir) broadband sensor that was designed to study top-of-the-atmosphere (TOA) fluxes. MODIS and MISR have higher resolutions (< 1 km), enabling better study of clouds and aerosols. MODIS has a larger horizontal swath, but MISR can address angular information [2]. MODIS and MISR data, averaged to CERES resolution, can help interpret CERES data as a function of clouds and aerosols. In fact, the CERES team has done merging of MODIS onto the CERES footprint, and this data set is called the CERES Single Scanner Footprint (SSF) product [3]. Level 1B MISR data have also been merged onto CERES SSF [4] but is not fully operational. In this paper, we combine both MODIS and MISR level 2 with CERES SSF data.

There are several data streams and products that are useful for atmospheric aerosol, cloud, and radiation budget research. In this paper, we focus primarily on examples related to the study of aerosols. The fundamental data product from satellite sensors are geo-referenced calibrated radiances at the sensors’ original resolution. These data are known as level 1B. Retrieved geophysical parameters are known as level 2 and are usually derived at predefined spatial resolutions (e.g., 10 km² for MODIS aerosol retrieval). Level 3 data are products provided on a regular latitude/longitude grid (e.g., 1 × 1° for MODIS aerosols). Each of these data is suited for different applications, ranging from image-based classification to validation/intercomparisons, to scientific applications such as the study of aerosol radiative forcing and assimilation into global climate models.

Several scientific questions related to air quality and radiative effects of aerosols, can be addressed using merged aerosol and

Manuscript received May 24, 2007; revised September 18, 2007. This work was supported in part by the National Aeronautics and Space Administration (NASA)’s Radiation Sciences, by Interdisciplinary Science, by an Earth Observing System grant, and by Atmospheric Chemistry Modeling and Analysis Programs. The work of P. Gupta was supported by NASA Headquarters under the Earth and Space Science Fellowship (NESSF) grant.

The authors are with the Department of Atmospheric Sciences, University of Alabama in Huntsville, Huntsville, AL 35899 USA (e-mail: sundar@nsstc.uah.edu).

Color versions of one or more of the figures in this paper are available online at <http://ieeexplore.ieee.org>.

Digital Object Identifier 10.1109/TGRS.2008.916087

93 radiation level 2 data products. Specifically, the combination of
94 MODIS, MISR, and CERES can help estimate aerosol radiative
95 effects. Until recently, MODIS aerosol products were not de-
96 rived over bright targets such as deserts. While the MODIS deep
97 blue algorithm [19], [20] now provides aerosol retrievals over
98 bright surfaces, it is not yet fully evaluated and has not yet been
99 fully processed for all Terra-MODIS data. MISR data, on the
100 other hand, have been validated over bright surfaces [5]. Since
101 MISR is limited in horizontal swath, as compared to MODIS,
102 but provides better retrievals in bright areas, it is desirable to
103 merge the two. While cross-sensor MODIS/MISR validation
104 [5] is not the focus of this paper, we use the MODIS and MISR
105 products together to estimate the aerosol properties for specific
106 cases (presented in Section IV).

107 It is generally believed that aerosols affect the climate sys-
108 tem significantly [6]. Since the launch of Terra and other
109 satellites, there is a shift from modeling-based assessments to
110 increasingly observational based approaches [7] for estimating
111 climate effects of aerosols. Another aspect of moving toward
112 an observational approach for studying aerosol radiative ef-
113 fects is the integration of energy budget (CERES) and imager
114 (MODIS/MISR) data sets from Terra [2], [8]. This method
115 provides an independent assessment of aerosol radiative effects,
116 which can be compared against modeling-based approaches.
117 While the CERES provides broadband TOA fluxes, multispec-
118 tral and multiangle measurements from MODIS and MISR
119 are needed to detect clouds and aerosols within the CERES
120 footprint and provide geophysical quantities such as aerosol
121 optical thickness (AOT) and particle size. Thus, combinations
122 of sensors can then be used to answer questions such as “What
123 is the radiative forcing of aerosols?” and “What is the radia-
124 tive forcing efficiency (aerosol forcing per unit optical depth),
125 and how does radiative forcing vary as a function of aerosol
126 properties?” The goal of this paper is to raise awareness of
127 multisensor data fusion to provide a framework for merging
128 level 2 aerosol data products at different spatial resolutions
129 and to finally provide some examples related to estimation of
130 aerosol radiative effects.

131 Data fusion can be defined as the merging of data from mul-
132 tiple sensors and related information from different databases
133 to achieve improved accuracy and more specific inferences [9].
134 Merging multiple satellite data sets utilizes the strengths of in-
135 dividual sensors, while constraining weaknesses of others. Past
136 research studies have successfully utilized merged satellite data
137 sets to assess landslide hazards using supervised classification
138 [12]. In the context of aerosol research, data fusion can be done
139 on different levels of data, such as radiance level 1B data [4],
140 geophysical parameters level 2 data (this paper), and gridded
141 level 3 data sets [10].

142 There are various issues related to data fusion, including
143 (but not limited to) data versions, error analysis of the indi-
144 vidual and the merged data products, and validation of these
145 products. For example, the CERES algorithm is processed at
146 NASA Langley with its own set of cloud and aerosol clearing
147 algorithms. MODIS aerosol product (MOD04) is generated at
148 the NASA Goddard Space Flight Center and then merged at
149 NASA Langley by the CERES science team called the CERES
150 SSF product. While the MODIS aerosol algorithm goes through

changes, and while newer versions are available (currently 151
collection 5), the CERES SSF product may not reflect the 152
MODIS product changes immediately due to data processing 153
timelines. The MISR level 2 data products that are developed 154
at the Jet Propulsion Laboratory are run routinely at NASA 155
Langley, although these products are not merged within the 156
CERES product routinely. Therefore, the best possible scenario 157
for independent users interested in data fusion is to obtain the 158
CERES SSF and merge the MISR aerosol products into the 159
CERES footprint, which is the focus of this paper. 160

161 II. DATA

In this section, we briefly describe the satellite sensors and 162
the data sets that are relevant to this paper. All of the data 163
sets are in hierarchical data format (hdf) and were obtained 164
through the NASA Langley Distributed Active Archive Center 165
(<http://eosweb.larc.nasa.gov>). The MODIS, MISR, and CERES 166
on Terra are in a polar-orbiting Sun-synchronous orbit at 167
705 km, with a descending equatorial crossing time of 168
10:30 A.M. The Terra satellite began collecting data in February 169
2000. Nearly 1 TB of global CERES, MODIS, and MISR data 170
were collected and processed for this research. 171

MODIS is a multispectral imaging radiometer that provide 172
measurements of the Earth’s land, ocean, and atmosphere with 173
36 spectral bands, covering the wavelength range from 0.405 to 174
14.385 μm with a swath width of 2330 km and providing global 175
coverage in 1–2 days [11]. The applicable MODIS data set in 176
this paper is the aerosol level 2 (collection 4) MOD04 products 177
at a 10-km² resolution, containing, among other parameters, the 178
AOT, the fine mode fraction, and the cloud fraction. A descrip- 179
tion of the MODIS aerosol retrieval algorithm and validation 180
strategies is fully explained in [12]. Table I shows some com- 181
monly used MODIS level 2 (MOD04) parameters for aerosol 182
research that are already merged within the CERES SSF files. 183

The MISR on Terra images the Earth in four spectral bands 184
(0.446, 0.557, 0.671, and 0.866 μm) and has nine push broom 185
cameras operating at nine different angles with a swath width 186
of about 360 km [13]. Due to the narrow swath width, near 187
global coverage is obtained only over 9 days at the equator and 188
2 days near the poles. There are 233 distinct repeating orbits 189
called paths, which are repeated every 16 days and are labeled 190
according to the Landsat Worldwide Reference System. To 191
simplify the processing and storing of these data over a large 192
geographical area, each MISR path is divided into a series 193
of predefined uniform-sized boxes along the ground track. 194
Each path is divided into 180 blocks, measuring 563.2 km 195
(cross-track) by 140.8 km (along-track). For a given path, a 196
numbered block always contains the same geographic location. 197

The relevant MISR data set for this paper is the level 2 198
aerosol data (MIL2ASAE), containing AOT at four spectral 199
channels, AOT values for three different size ranges of particles, 200
single-scattering albedo, and other related parameters (Table I). 201
These level 2 geophysical parameters are provided in a 202
17.6-km² spatial resolution. A detailed description of the 203
aerosol algorithm is given in [14]. Geographical information 204
on a Space Oblique Mercator (SOM) grid is given in the MISR 205
Ancillary Geographic Product (AGP). Geographical positions 206

TABLE I
SELECTED CERES SSF (INCLUDES MODIS AND CERES) AND MISR LEVEL 2 PARAMETERS COMMONLY USED IN AEROSOL RESEARCH

CERES SSF products	
1	CERES SW TOA flux
2	CERES LW TOA flux
3	CERES WN TOA flux
4	PSF-wtd MOD04 cloud fraction land
5	PSF-wtd MOD04 aerosol types land
6	PSF-wtd MOD04 corrected optical depth land (0.47, 0.55, 0.66)
7	PSF-wtd MOD04 cloud fraction ocean
8	PSF-wtd MOD04 effective optical depth average ocean (0.47, 0.55, 0.66, 0.86, 1.24, 1.64, 2.1)
9	PSF-wtd MOD04 optical depth small average ocean (0.55, 0.86, 2.1)
MISR level 2 aerosol products	
1	RegBestEstimateSpectralOptDepth (0.46, 0.55, 0.67, 0.86)
2	RegBestEstimateAngstromExponent
3	RegBestEstimateSpectralSSA (0.46, 0.55, 0.67, 0.86)
4	RegBestEstimateSpectralOptDepthFraction
5	RegBestEstimateNumberFraction
6	RegBestEstimateVolumeFraction

207 of MISR pixels in terms of latitude and longitude are provided
208 in a 1.1-km² grid resolution and stored in separate files for
209 each fixed MISR orbit. These 233 files corresponding to 233
210 distinct MISR orbits provided as separate parameters can be
211 used to geolocate the level 2 data products (Table I).

212 The CERES provides broadband radiative energy measure-
213 ments at the TOA, both in the long and short waves [15]. Each
214 CERES instrument has three channels: 1) a short-wave channel
215 for measuring reflected sunlight (0.3–5 μm); 2) a long-wave
216 channel for measuring Earth-emitted thermal radiation in the
217 8–12- μm “window” region; and 3) a total channel for radiation
218 between 0.3 and 200 μm . The Terra carries two identical
219 CERES instruments: one operates in a cross-track scan mode
220 (FM-1) and the other in a biaxial scan mode (FM-2) for
221 developing angular models to convert the measured broadband
222 radiances to fluxes. On Terra, the CERES has a spatial resolu-
223 tion of approximately 20 km² (equivalent diameter) at nadir.

224 For each CERES footprint, the MODIS AOT and other
225 relevant aerosol information from MODIS are convolved using
226 point spread functions (PSFs) and matched in space and time to
227 the CERES measurement [16] and are available as the CERES
228 SSF product. Therefore, for each CERES footprint, the PSF-
229 weighted cloud fraction and aerosol properties such as optical
230 depth are provided only from the MODIS data. The CERES
231 SSF data can be ordered online for user-selected regions and
232 parameters of interest. There are 160 parameters for each pixel,
233 ranging from geolocation information, Sun–satellite geometry,
234 cloud and aerosol information, and CERES radiative energy
235 fluxes (Table I).

236 For illustrative purposes, Fig. 1 shows an example of an
237 aerosol event observed by the three different sensors from Terra
238 on October 26, 2003. Fig. 1(a) shows a true-color composite
239 of channel 0.67 μm in red, channel 0.55 μm in green, and
240 channel 0.47 μm in blue around the west coast of the U.S.
241 from the MODIS level 1B data. Fig. 1(b) shows the MISR
242 (version F03, V002 data) data for the same day using similar
243 bands as MODIS. Both MODIS and MISR clearly show the
244 large smoke plumes from the west coast of California. The
245 CERES short-wave flux is shown in Fig. 1(c) from this period,
246 and the image appears blocky when compared to the MODIS

and MISR imagery due to the large pixel size of the CERES
247 scanner. Note the large swath width of the MODIS and CERES
248 when compared to the MISR. Dark areas correspond to ocean
249 background, whereas smoke plumes from the fires and the
250 clouds appear brighter due to higher reflectivity when compared
251 to the background. This difference in contrast between the
252 background and aerosols is used to separate aerosols and clouds
253 and is further used to retrieve aerosol properties by the MODIS
254 and MISR algorithms. The corresponding level 2 MODIS and
255 MISR (version F09, V002) AOT images are shown in Fig. 2(a)
256 and (b), respectively. MODIS uses multispectral methods, state-
257 of-the-art cloud clearing techniques, and predefined aerosol
258 models to retrieve the AOT value at 10 km² [12]. On the other
259 hand, MISR uses multispectral multiangle information and pre-
260 defined aerosol models to provide AOT retrievals over 17.6 km²
261 [14]. Both algorithms continue to undergo developments and
262 refinements with intensive validation against ground and
263 suborbital measurements. The CERES can be used directly to
264 obtain TOA short-wave fluxes due to smoke aerosols, provided
265 the aerosols can be identified using MODIS and MISR data.
266 This multisensor combination is powerful for studying aerosol
267 radiative effects from an observational perspective [2]. 268

III. METHODOLOGY

269

270 One of the goals of this paper is to demonstrate fusion of
271 CERES SSF and MISR level 2 aerosol products and show some
272 selected examples related to aerosol research. To merge MISR
273 level 2 aerosol (MIL2ASAE) products with CERES SSF (FM1,
274 Edition2B) in space and time, a collocation algorithm is first
275 developed. Since the three sensors are all on the same satellite,
276 collocation by time is simple.

277 A simple flowchart of the algorithm is shown in Fig. 3,
278 and since handling MISR data sets is not straightforward, the
279 methodology is described in detail. Each CERES SSF file
280 includes all geophysical parameters (such as TOA short- and
281 long-wave fluxes), geolocation information, and Sun–satellite
282 geometry, along with MODIS spectral AOTs and the MODIS
283 cloud fraction within each CERES footprint. There are about
284 160 parameters in the CERES SSF file, and any of these

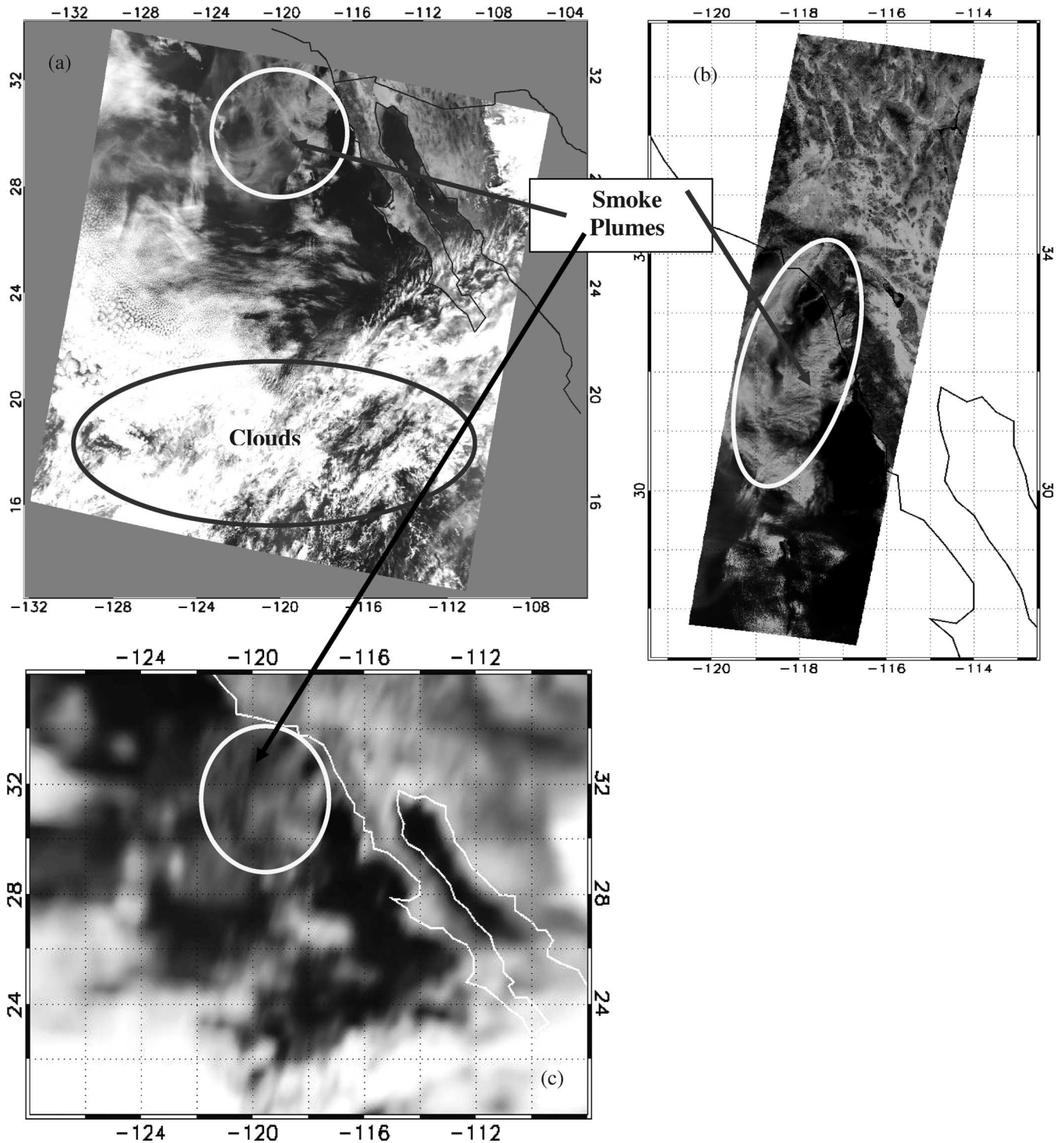


Fig. 1. True-color image of biomass burning event in the western U.S. on October 26, 2003, at 1840 GMT from (a) Terra-MODIS, (b) MISR nadir view, and (c) CERES short-wave flux.

285 parameters in combination with the MISR products can be
 286 obtained from our general-purpose software. The CERES
 287 SSF files contain data for a 1-h observation period, and
 288 date-time information is part of the filename. A typical
 289 CERES SSF file is named CER_SSF_Terra-FM1-MODIS_
 290 Edition2B_YYYYMMDDHH.hdf from the Terra satellite
 291 where CER indicates CERES, FM1 denotes that the data are
 292 from the cross-track scanner, and YYYY, MM, DD, and HH
 293 are the year, month, day, and hour, respectively.

The MISR products do not contain geolocation information
 294 such as latitude and longitude in the same file. However, the
 295 new data ordering tools provide some options to the user to add
 296 this information in the data file. The geolocation information
 297 is fixed for the 233 predefined MISR orbits and is available as
 298 separate files. The typical file naming of the geolocation file
 299 is MISR_AM1_AGP_Pathnumber_F01_24.hdf. Similar to the
 300 CERES SSF, the MISR data files contain many parameters,
 301 including spectral AOT, single-scattering albedo, Angstrom
 302

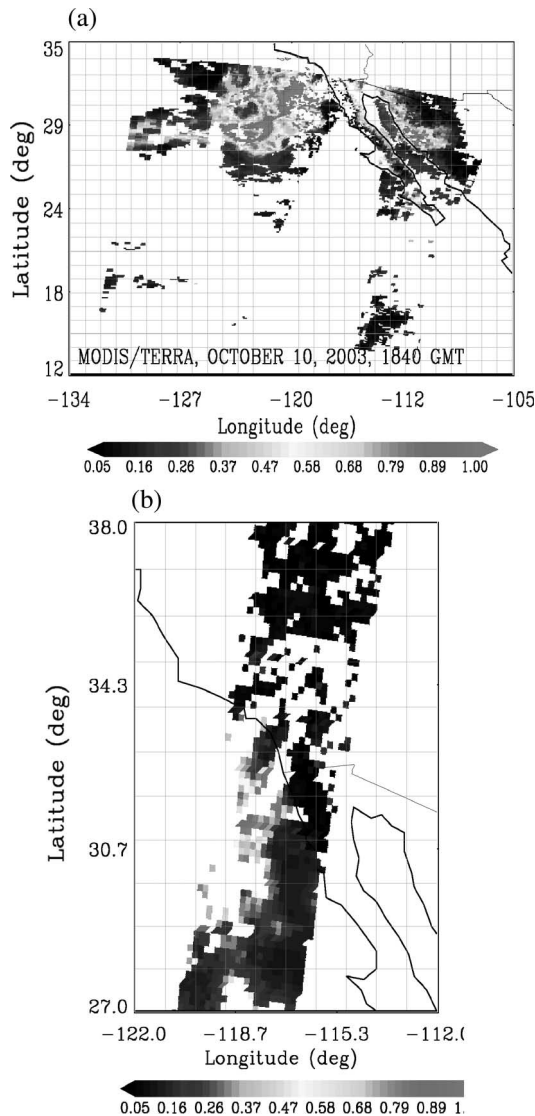


Fig. 2. Midvisible AOT from level 2 aerosol products from (a) MODIS and (b) MISR for the images shown in Fig. 1. Missing values in AOT are due to clouds.

303 coefficient, and size-fractioned AOTs. A total of 121 parameters
 304 are available from the MISR aerosol product, and our software
 305 is flexible enough to accommodate any combination of these
 306 parameters to be collocated with CERES SSF in space and time.
 307 Although each MISR path contains 180 blocks, due to seasonal
 308 variations in the portion of the Earth that is in daylight, only
 309 up to 142 blocks contain valid data points. Valid MISR aerosol
 310 retrieval blocks are identified using start and end block numbers
 311 provided in the data file. Then, the date and time parameters
 312 are obtained for the same blocks. The MISR does not provide
 313 date and time for each pixel, but it provides information for
 314 the center of each block. Interpolation is performed to obtain
 315 the time information for each pixel within a given block. MISR
 316 latitude and longitude data are in a 1.1-km² resolution, whereas
 317 MISR aerosol products are in a 17.6-km² resolution. For each
 318 valid data pixel, the corresponding latitude and longitude is
 319 obtained by selecting the center latitude and longitude of the
 320 box of 16 × 16 pixels in geolocation data.

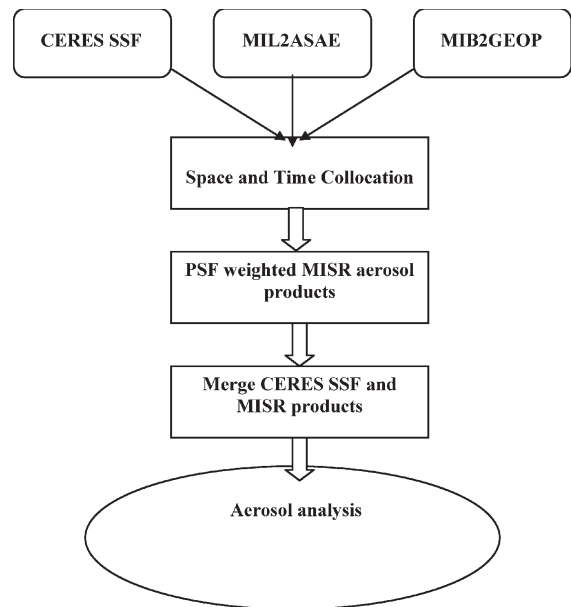


Fig. 3. Flowchart of the space and time collocation between the CERES SSF and MISR level 2 products. The CERES SSF product contains the CERES and merged MODIS data, and MIL2ASAE and MIB2GEOP are the MISR aerosol product data set and the geolocation files, respectively.

The main collocation algorithm is divided into two sections. The first section deals with collocation in time, whereas the second deals with collocation in space. Since both the CERES and the MISR are onboard Terra, they provide near-simultaneous observations. The key issue in time collocation is how to find the appropriate MISR file corresponding to the CERES observation period, and this is done by checking both day and time information. Since the MISR filename does not have date–time information, this becomes a cumbersome process. To increase searching efficiency, a separate database of date and time corresponding to the various orbits and path numbers are used to select the proper file corresponding to each CERES file. On proper selection of MISR file, the CERES SSF observation date and time information is matched with the MISR date/time, and then, the collocation in space begins. Since the sensors are on the same satellite, the observation time is almost the same, and therefore, temporal collocation is not necessary. To make the computer code more efficient and useful to the users, spatial collocation is performed only over the user-selected area of interest, which can be input to the algorithm by providing the latitude and longitude of the four corners of a region. Since the CERES and MISR have different ground resolutions, exact or one-to-one collocation in space may not be possible. Another important thing to note is the CERES pixel size, which can be larger than 100 km² at the edge of the CERES swath due to panoramic distortion, is an important factor when collocating MODIS and CERES. However, since the MISR swath is narrow, and it is in the middle of the CERES swath, panoramic distortion in the MISR is not significant.

The CERES pixel shape and size is not fixed, and it is therefore difficult to define its size parameters. Our algorithm uses two different averaging methods: one is simple arithmetic-weighted average, and the other one uses the CERES PSF average. In the first method, the CERES pixel is assumed to be

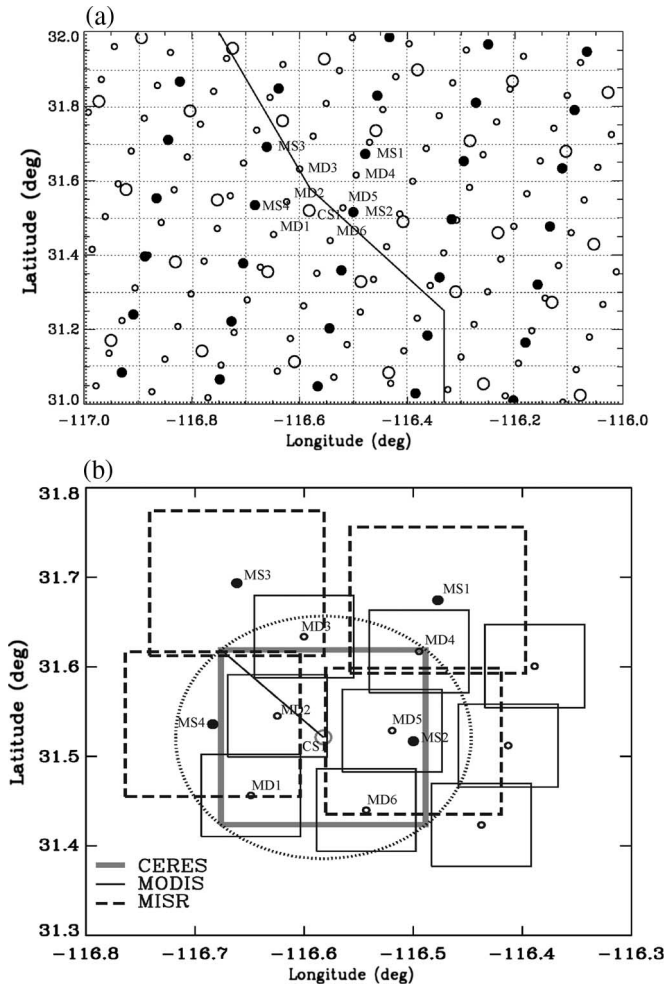


Fig. 4. (a) Latitude and longitude of MISR, MODIS, and CERES pixels for a small portion of the swath and (b) the collocation of one CERES pixel with multiple MISR pixels. The location of the CERES pixel is shown by a large unfilled circle, MODIS by a small unfilled circle, and MISR pixel by a medium filled circle. The CERES pixel CS1 in (a) is shown in greater detail in (b). The MODIS pixels are labeled MD, and the MISR pixels are labeled MS.

355 rectangular with one edge as defined by along-track dimension
 356 and with the other edge as defined by across-track length,
 357 although other shape functions can easily be accommodated.
 358 The second method uses PSF to map the MISR data to the
 359 CERES pixel. Fig. 4(a) shows a small section of the MODIS,
 360 MISR, and CERES swath, indicating the relative size of each
 361 pixel, as well as the collocation procedure. Both along- and
 362 across-track lengths for each rectangular pixel are calculated
 363 using viewing zenith angle information, and correction due
 364 to the Earth's curvature is also made. Fig. 4(b) shows the
 365 collocation procedure for one CERES pixel (CS1) and the
 366 corresponding MODIS (MD) and MISR (MS) pixels. The size
 367 of each MODIS, MISR, and CERES pixel is indicated and is
 368 approximately equal to the dimensions at nadir [Fig. 4(b)]. The
 369 circle denotes the search radius used in calculating mean MISR
 370 values from all the pixels falling within the CS1 pixel.

371 To obtain the MISR product value at CERES pixel location
 372 and resolution, the spherical distance that accounts for the
 373 curvature of the Earth between the MISR and CERES pixel is
 374 calculated. All the MISR pixels falling within the circle with
 375 the radius that is half of the diagonal of the CERES pixel are

averaged using two different methods. The first method uses the 376
 arithmetic average of all MISR parameters (e.g., AOT) falling 377
 within the circle. The second uses the distance weighted aver- 378
 age, where all the MISR pixels falling within the CERES circle 379
 receive a weight between 0 and 1 based on how close it is from 380
 the center of the CERES pixel. There are numerous weighting 381
 function options that are available, and we used the inverse 382
 distance weighting, where weights are a decreasing function of 383
 distance. The third option (second averaging approach) used is 384
 the CERES PSF weighted average [17] value of MISR AOT 385
 at the CERES footprint. The CERES convolution algorithm 386
 weights the MISR pixel based on where it is located within the 387
 CERES pixel [4]. 388

IV. APPLICATION OF MERGED MODIS-MISR-CERES DATASETS 389 390

We provide three selected examples of the collocated aerosol 391
 and flux data from MODIS, MISR, and CERES over three 392
 different regimes [Fig. 5(a)–(e)]. Also included in one case 393
 study is the comparison of the MISR AOT with ground-based 394
 sunphotometer values. 395

A. MISR, MODIS, and AERONET AOT 396

Fig. 5(a) shows the level 2 AOT from the MODIS and 397
 MISR over the Sahara Desert for January 16, 2006. Two whole 398
 MODIS swaths and a partial swath show the large MODIS 399
 coverage over this area. Note that the MODIS AOT retrievals 400
 are only available over cloud-free vegetated surfaces (dark 401
 target) and, therefore, are restricted to latitudes between 0° N 402
 and 15° N in the area of study, and no retrievals are available 403
 in the desert regions shown in gray color. The MISR, on the 404
 other hand, has three narrow swaths during this day but has 405
 complete aerosol retrievals over all surface types, except in 406
 cloudy conditions that can be used to fill in AOT values where 407
 MODIS retrievals are not available. Also shown in black dots 408
 are several Aerosol Robotic Network (AERONET) locations 409
 that are currently the standard for validating aerosol retrievals. 410
 Comparisons between satellite retrievals and AERONET loca- 411
 tions are important for testing the robustness of the satellite 412
 retrievals. An intercomparison of the MISR 17.6-km² AOT 413
 retrievals with ± 30 min of AOT values from AERONET is 414
 shown in Fig. 5(b). This intercomparison is performed on all the 415
 AERONET stations shown in Fig. 5(a) during January to March 416
 2006. An excellent correlation between the two retrievals indi- 417
 cates the high quality of the MISR retrievals over bright targets 418
 such as deserts and is especially useful in these areas where 419
 MODIS retrievals are not possible. 420

B. Use of MODIS, MISR, and CERES for Estimating LWRE 421

Including MISR into the CERES SSF product will enable 422
 us to estimate TOA long-wave radiative effect (LWRE) as a 423
 function of aerosol properties even over bright surfaces. The 424
 LWRE is defined as the difference in CERES TOA long-wave 425
 fluxes with and without the presence of aerosols. Fig. 5(c), 426
 which was adapted from [2], shows the spatial distribution of 427
 MISR AOT for September 2000 over the Sahara Desert [2]. In 428

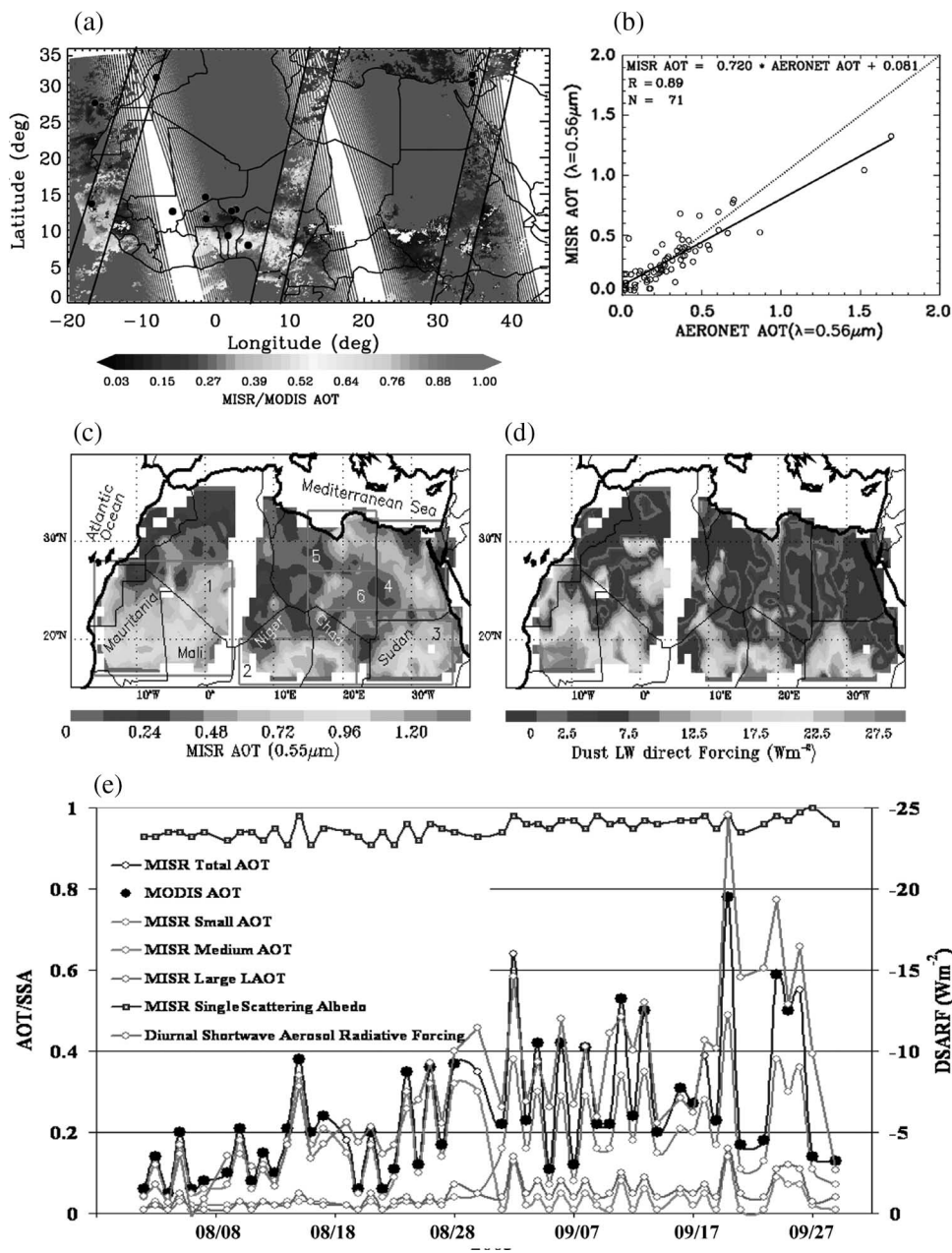


Fig. 5. Case studies of data fusion. (a) Spatial distribution of MISR and MODIS derived AOT on January 16, 2006 over North Africa. (b) MISR AOT versus AERONET AOT. (c) MISR AOT for September 2004. (d) CERES-derived long-wave dust aerosol radiative effect (from [2]). (e) Time series of MODIS- and MISR-derived aerosol properties, along with the CERES biomass burning aerosol effect over the Amazon basin during August and September 2003.

429 the Sahara Desert regions, MODIS retrievals were not available,
 430 and therefore, the MISR AOT values were used in conjunction
 431 with the CERES data for addressing dust radiative effects.
 432 MODIS cloud information was used to remove cloud contam-
 433 ination within the CERES pixel since the MODIS offers more
 434 channels and a higher spatial resolution to detect clouds. During
 435 this month, closer to the equator, biomass burning activities are
 436 responsible for the high AOT observed in this region. Away
 437 from the equator, dust aerosols increase the AOT, and several re-
 438 gions labeled 1–6 in Fig. 5(c) indicate the high AOT that MISR
 439 retrieves. The collocated MODIS–MISR–CERES data sets can
 440 then be used to address the effects of dust aerosols on the radia-
 441 tive balance of the Earth–atmosphere system. Fig. 5(d) shows
 442 the long-wave TOA dust aerosol radiative forcing. Positive

aerosol LWRE values indicate that the aerosols emit at a colder
 443 temperature when compared to the Earth’s surface, thereby
 444 reducing the amount of Earth-emitted radiation back to space,
 445 thereby creating a “warming effect” that is opposite in effect
 446 to that of the short-wave reflective nature of other aerosols [2].
 447 This example clearly shows the potential of using MODIS and
 448 MISR aerosol properties over bright targets along with CERES
 449 observations, which is not possible by using one sensor alone. 450

C. Use of MODIS, MISR, and CERES for Studying Biomass Burning Aerosols 451
 452

We move from a highly reflective background in Africa, 453
 where dust is prevalent, to another example over South 454

455 America, where the reflectivity is low and where biomass burn-
 456 ing aerosols are prevalent. In South America, each year during
 457 the dry season, agricultural activities result in several teragrams
 458 of smoke aerosols that are released into the atmosphere. These
 459 aerosols affect the regional radiative balance significantly.
 460 MODIS and MISR can be used to map the spatial distribution of
 461 aerosols. Retrieved AOT and aerosol properties from MISR can
 462 be used to further study aerosol forcing as a function of various
 463 aerosol properties. Fig. 5(e) presents the time series of aerosol
 464 properties from MISR and short-wave forcing over the Amazon
 465 basin (20° S–0° N and 65° S–45° S) during August and
 466 September 2003 estimated using merged MODIS–MISR–
 467 CERES data sets. Again, cloud clearing of CERES pixels has
 468 been done using MODIS data. MISR retrieval produces aerosol
 469 parameters, including the AOT due to small-, medium-, and
 470 large-sized particles, as well as the total AOT at 0.55 μm ,
 471 along with single-scattering albedo and Angstrom coefficient.
 472 The short-wave forcing is the difference in the TOA short-wave
 473 flux between clear and aerosol regions, which is an important
 474 parameter for climate research.

475 This time series shows diurnally averaged short-wave aerosol
 476 radiative forcing (DSARF) and the associated aerosol proper-
 477 ties. The DSARF is defined as the difference between clear-
 478 sky (F_{clr}) and aerosol-sky fluxes (F_{aero}) that is adjusted for
 479 diurnal effects [22]. F_{clr} corresponds to cloud- and aerosol-
 480 free fluxes, while F_{aero} corresponds to cloud-free fluxes from
 481 regions where aerosols are present [2]. Here, it is important
 482 to note that during August and September, the study region in
 483 South America is dominated by anthropogenic biomass burning
 484 aerosols, and hence, the term “radiative forcing” is used instead
 485 of “radiative effects” [7].

486 Fig. 5(e) clearly shows that both AOT and DSARF increases
 487 from August to September, which was mainly due to the
 488 increase in biomass burning activities in the region. Also, the
 489 AOTs due to medium-sized particles contribute more in total
 490 AOT during August, but small mode contribution is more in
 491 September compared to any other size mode. For comparison,
 492 the MODIS total AOT is shown as black dots, and it compares
 493 remarkably well with the MISR total AOT shown in blue over
 494 this region. Further analysis is provided in Patadia *et al.* [18]
 495 who quantitatively discuss what portion of the AOT and forcing
 496 comes from various particle sizes. Collocated data sets such as
 497 these can be used to further improve our understanding of the
 498 role of aerosols on the energy balance of the Earth–atmosphere
 499 system.

500

V. SUMMARY

501 There are many satellite sensors that are currently in orbit
 502 for studying the Earth–atmosphere in an integrated fashion.
 503 However, most studies to date largely focus upon single-sensor
 504 approaches for studying specific problems. This is largely
 505 due to the complexities in merging data and the volume of
 506 data involved. There are various methods for merging data at
 507 different processing levels. While some applications require
 508 merging of radiance level data (level 1), this could often be
 509 time consuming and laborious. However, there are a variety
 510 of retrieved products (level 2) at different spatial and temporal

resolutions that could be merged to address scientific issues. 511
 While the ideal scenario is to have a unified cloud-clearing 512
 algorithm across all sensors and then retrieve aerosol properties 513
 and convolve it within the CERES footprint, this is not the 514
 current practice. Therefore, some of the product level data 515
 fusion has to be done by individual researchers. 516

In this paper, we have combined three data sets, namely, 517
 the MODIS, the MISR, and the CERES for studying common 518
 problems in aerosol research. Note that the MODIS and CERES 519
 have already been merged at NASA Langley (the CERES SSF 520
 product). We merge the level 2 MISR aerosol product with 521
 the CERES SSF data. Each data set has numerous retrieved 522
 parameters and different algorithms for creating these param- 523
 eters. We have not attempted to discuss the algorithms, the 524
 retrievals, or the accuracies since they are not the focus of 525
 this paper. Our major goal has been to raise the awareness of 526
 multisensor data fusion from sensors on a single satellite and 527
 provide a simple framework for merging data. In the process, 528
 we have also provided some selected examples. These are not 529
 meant to be exhaustive by any means. However, our examples 530
 indicate the robustness of the data fusion methods and value- 531
 added information, since the geophysical parameters such as 532
 AOT and short- and long-wave forcing are consistent with other 533
 research studies. We now have software in place that can be 534
 used to merge these types of data sets for aerosol and possibly 535
 cloud research. With the series of satellites as part of the 536
 A-train that will obtain data over a pixel within seconds to 537
 several minutes of each other, collocation issues could be 538
 challenging, and further research is necessary to merge data 539
 from multiple satellites for addressing research questions. 540

ACKNOWLEDGMENT

541
 The authors would like to thank the Atmospheric Sciences 542
 Data Center at the NASA Langley Research Center, from which 543
 the data were obtained. 544

REFERENCES

- 545
 [1] G. Asrar and J. Dozier, *EOS: Science Strategy for the Earth Observing* 546
System. New York: AIP, 1994. 547
 [2] J. Zhang and S. A. Christopher, “Longwave radiative forcing of dust 548
 aerosols over the Saharan Desert estimated from MODIS, MISR, and 549
 CERES observations from Terra.” *Geophys. Res. Lett.*, vol. 30, no. 23, 550
 2188, 2003. DOI: 10.1029/2003GL018479. 551
 [3] E. B. Geier, R. N. Green, D. P. Kratz, P. Minnis, W. F. Miller, 552
 S. K. Nolan, and C. B. Franklin, *Single Satellite Footprint TOA/Surface* 553
Fluxes And Clouds (SSF) Collection Document. Hampton, VA: NASA 554
 Langley Res. Center, 2001. [Online]. Available: [http://asd-www.larc.](http://asd-www.larc.nasa.gov/ceres/collect_guide/SSF_CG.pdf) 555
[nasa.gov/ceres/collect_guide/SSF_CG.pdf](http://asd-www.larc.nasa.gov/ceres/collect_guide/SSF_CG.pdf) 556
 [4] N. G. Loeb, W. Sun, W. F. Miller, K. Loukachine, and R. Davies, “Fu- 557
 sion of CERES, MISR, and MODIS measurements for top-of-atmosphere 558
 radiative flux validation,” *J. Geophys. Res.*, vol. 111, no. D18, D18209, 559
 2006. DOI: 10.1029/2006JD007146. 560
 [5] W. A. Abdou, D. J. Diner, J. V. Martonchik, C. J. Bruegge, R. A. Kahn, 561
 B. J. Gaitley, K. A. Crean, L. A. Remer, and B. Holben, “Compari- 562
 son of coincident Multiangle Imaging Spectroradiometer and Moderate 563
 Resolution Imaging Spectroradiometer aerosol optical depths over land 564
 and ocean scenes containing aerosol robotic network sites,” *J. Geophys.* 565
Res.—Atmos., vol. 110, no. D10, pp. 11 967–11 976, 2005. D10S07. 566
 [6] M. Bellouin, O. Boucher, J. Haywood, and M. S. Reddy, “Global estimate 567
 of aerosol direct radiative forcing from satellite measurements,” *Nature*, 568
 vol. 438, no. 7071, pp. 1138–1141, Dec. 2005. 569
 [7] T. L. Anderson, R. J. Charlson, N. Bellouin, O. Boucher, M. Chin, 570
 S. A. Christopher, H. J. Haywood, Y. J. Kaufman, S. Kinne, J. Ogren, 571

- 572 L. A. Remer, T. Takemura, D. Tanre, O. Torres, C. R. Trepte,
573 B. A. Wielicki, D. Winker, and H. Yu, "An A-Train strategy for quan-
574 tifying direct climate forcing by anthropogenic aerosols," *Bull. Amer.*
575 *Meteorol. Soc.*, vol. 86, no. 12, pp. 1795–1809, 2005.
- 576 [8] S. A. Christopher and J. Zhang, "Cloud-free shortwave aerosol radiative
577 effect over oceans: Strategies for identifying anthropogenic forcing
578 from Terra satellite measurements," *Geophys. Res. Lett.*, vol. 31, no. 18,
579 L18 101, 2004. DOI: 10.1029/2004GL020510.
- 580 [9] L. Wald, "Some terms of reference in data fusion," *IEEE Trans. Geosci.*
581 *Remote Sens.*, vol. 37, no. 3, pp. 1190–1193, May 1999.
- 582 [10] J. Acker and G. Leptoukh, "Online analysis enhances use of NASA Earth
583 science data," *Eos Trans. AGU*, vol. 88, no. 2, pp. 14–17, 2007.
- 584 [11] P. E. Ardanuy, D. Han, and V. V. Salomonson, "The Moderate Resolution
585 Imaging Spectrometer (MODIS) science and data system requirements,"
586 *IEEE Trans. Geosci. Remote Sens.*, vol. 29, no. 1, pp. 75–88, Jan. 1991.
- 587 [12] L. A. Remer, Y. J. Kaufman, D. Tanré, S. Mattoo, D. A. Chu, J. V. Martins,
588 R.-R. Li, C. Ichoku, R. C. Levy, R. G. Kleidman, T. F. Eck,
589 E. Vermote, and B. N. Holben, "The MODIS aerosol algorithm, products
590 and validation," *J. Atmos. Sci.*, vol. 62, no. 4, pp. 947–973, Apr. 2005.
- 591 [13] D. J. Diner, J. C. Beckert, G. W. Bothwell, and J. I. Rodriguez, "Per-
592 formance of the MISR instrument during its first 20 months in Earth
593 orbit," *IEEE Trans. Geosci. Remote Sens.*, vol. 40, no. 7, pp. 1449–1466,
594 Jul. 2002.
- 595 [14] R. Kahn, B. Gaitley, J. Martonchik, D. Diner, K. Crean, and B. Holben,
596 "Multiangle Imaging Spectroradiometer (MISR) global aerosol optical
597 depth validation based on two years of coincident AERONET observa-
598 tions," *J. Geophys. Res.—Atmos.*, vol. 110, no. D10, D10S04, 2005. DOI:
599 j0004706R.
- 600 [15] B. A. Wielicki, B. R. Barkstrom, E. F. Harrison, R. B. Lee, III,
601 G. L. Smith, and J. E. Cooper, "Clouds and the Earth's radiant energy
602 system (CERES): An Earth Observing System experiment," *Bull. Amer.*
603 *Meteorol. Soc.*, vol. 77, no. 5, pp. 853–868, May 1996.
- 604 [16] G. L. Smith, "Effects of time response on the point spread function
605 of a scanning radiometer," *Appl. Opt.*, vol. 33, no. 30, pp. 7031–7037,
606 Oct. 1994.
- 607 [17] R. N. Green and B. A. Wielicki, *Convolution of Imager Cloud Prop-*
608 *erties With CERES Footprint Point Spread Function (Subsystem 4. 4),*
609 *Clouds and the Earth's Radiant Energy System (CERES) Algorithm*
610 *Theoretical Basis Document*. Hampton, VA: NASA Langley Res.
611 Center, 1996. [Online]. Available: [http://asd-www.larc.nasa.gov/ATBD/](http://asd-www.larc.nasa.gov/ATBD/ATBD.html)
612 [ATBD.html](http://asd-www.larc.nasa.gov/ATBD/ATBD.html)
- 613 [18] F. Patadia, P. Gupta, S. A. Christopher, and J. S. Reid, "A multi-year data
614 fusion approach for assessing biomass burning aerosol radiative impacts
615 over Amazonia," *J. Geophys. Res.*, 2008. DOI:10.1029/2007JD009486.
- 616 [19] N. C. Hsu, S. C. Tsay, M. D. King, and J. R. Herman, "Aerosol properties
617 over bright-reflecting source regions," *IEEE Trans. Geosci. Remote Sens.*,
618 vol. 42, no. 3, pp. 557–569, Mar. 2004.
- 619 [20] N. C. Hsu, S. C. Tsay, M. D. King, and J. R. Herman, "Deep blue
620 retrievals of Asian aerosol properties during ACE-Asia," *IEEE Trans.*
621 *Geosci. Remote Sens.*, vol. 44, no. 11, pp. 3180–3195, Nov. 2006.
- 622 [21] Y.-L. Chang, L.-S. Liang, C.-C. Han, J.-P. Fang, W.-Y. Liang, and
623 K.-S. Chen, "Multisource data fusion for landslide classification using
624 generalized positive Boolean functions," *IEEE Trans. Geosci. Remote*
625 *Sens.*, vol. 45, no. 6, pp. 1697–1708, Jun. 2007.
- 626 [22] L. A. Remer and Y. J. Kaufman, "Aerosol effect on the distribution of
627 solar radiation over the clear-sky global oceans derived from four years of
628 MODIS retrievals," *Atmos. Chem. Phys. Discuss.*, vol. 5, no. 4, pp. 5007–
629 5038, 2005.



Pawan Gupta received the M.Sc. degree in physics 630
from Devi Ahilya University, Indore, India, in 631
2000 and the M.Tech. degree in space and at- 632
mospheric sciences from the Physical Research Lab- 633
oratory, Ahmedabad, India, and Andhra University, 634
Visakhapatnam, India, in 2003. He is currently work- 635
ing toward the Ph.D. degree in atmospheric science 636
at the University of Alabama, Huntsville. 637

From 2002 to 2003, he was a Junior Research 638
Fellow at the National Remote Sensing Agency, 639
Hyderabad, India. In 2005, he received NASA's 640
Graduate Student Fellowship in Earth Systems Science. His current research 641
interests mainly include the study of atmospheric aerosols, satellite remote 642
sensing of aerosols and particulate matter air quality, Earth-atmosphere ra- 643
diation budget, and data fusion from multiple satellite and surface based 644
instruments. 645



Falguni Patadia received the M.Sc. degree in 646
physics from Devi Ahilya University, Indore, 647
India, in 2000 and the M.Tech. degree in space and 648
atmospheric sciences from the Physical Research 649
Laboratory, Ahmedabad, India, and Andhra Univer- 650
sity, Visakhapatnam, India, in 2003. She is currently 651
working toward the Ph.D. degree in atmospheric 652
science at the University of Alabama in Huntsville. 653

Her current research interests mainly include the 654
study of atmospheric aerosols, satellite remote sens- 655
ing of aerosols, and data fusion of multiple satellite 656
and surface-based measurements for studying the role of tropospheric aerosols 657
on Earth's radiation budget. 658



Sundar A. Christopher received the Ph.D. degree 659
in atmospheric sciences from Colorado State Uni- 660
versity, Fort Collins, in 1995. He received the M.S. 661
degree in meteorology from the South Dakota School 662
of Mines and Technology, Rapid City, and the M.S. 663
degree in industrial/organizational psychology from 664
the University of Alabama, Huntsville (UAH). 665

He is currently a Professor in the Department of 666
Atmospheric Sciences and the Associate Director 667
of the Earth System Science Center at UAH. His 668
research interests include satellite remote sensing of 669
clouds and aerosols and their impact on air quality and global and regional 670
climate. 671